LIQUID CRYSTAL ON SILICON NON-MECHANICAL STEERING OF A LASER VIBROMETER SYSTEM

THESIS

Kevin S. Kuciapinski, Captain, USAF

AFIT/GSS/ENP/05-01

DEPARTMENT OF THE AIR FORCE
AIR UNIVERSITY

AIR FORCE INSTITUTE OF TECHNOLOGY

Wright-Patterson Air Force Base, Ohio

AFIT/GSS/ENP/05-01

LIQUID CRYSTAL ON SILICON NON-MECHANICAL STEERING OF A LASER
VIBROMETER SYSTEM

THESIS

Presented to the Faculty

Department of Engineering Physics

Graduate School of Engineering and Management

Air Force Institute of Technology

Air University

Air Education and Training Command

In Partial Fulfillment of the Requirements for the

Degree of Master of Science (Space Systems)

Kevin S. Kuciapinski, BS

Captain, USAF

September 2005

APPROVED FOR PUBLIC RELEASE; DISTRIBUTION UNLIMITED.

AFIT/GSS/ENP/05-01

LIQUID CRYSTAL ON SILICON NON-MECHANICAL STEERING OF A LASER
VIBROMETER SYSTEM

Kevin S. Kuciapinski, BS
Captain, USAF

Approved:
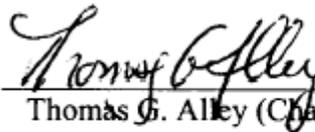
_____   _____
Thomas G. Alley (Chairman)   19 Sep '05
                      date
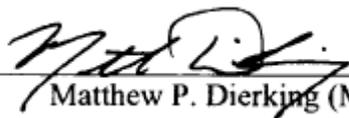
_____   _____
Matthew P. Dierking (Member)   19SEP05
                      date
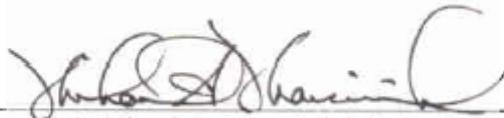
_____   _____
Michael A. Marciniak (Member)   19 Sep05
                      date

_____   _____
John F. McCalmont (Member)   19 Sep 05
                      date

AFIT/GSS/ENP/05-01

Abstract

This research examined the possibility of using a non-mechanical beam steering device to steer the beam of a coherent laser radar system. Non-mechanical beam steering devices offer many advantages in size, weight, power requirements, and steering speeds. Additionally, non-mechanical beam steering devices present the capabilities of splitting a single beam into multiple beams as well as beam forming and expanding. The current steering systems use bulky and maintenance intensive mirror and gimbaled systems. The application of non-mechanical steering of sensor systems promises to increase the capability, fuel consumption, and loiter times of the sensor platforms implementing laser radars.

The coherent laser radar system used in this experiment was a Laser Vibrometer System. The laser vibrometer detects the Doppler shift of coherent laser light reflected from a target. The Doppler frequency shift is used to measure the vibration velocity along the axis of the laser beam.

The beam of the laser vibrometer was steered from 0 mrad to 3 mrad at 1 mrad increments in both the left and right direction using the LCOS device. The laser vibrometer was able to accurately measure a 2500 Hz vibration target on the steered vibrometry beam at all steered angles. The intensity of the 2500 Hz signal received was found to decrease as steering approached 3 mrad in both directions. During this experimentation a small amount of noise was found to be induced on the vibration signal by the LCOS device. The noise signal was determined to be consistent and predictable located at 60 Hz harmonics. As a result, the 60 Hz harmonic noise profile was subtracted to produce a very clear 2500 Hz signal.

After successful vibration measurements were accomplished along the steered beam, the LCOS device was used to split the vibrometry beam into 2 separate beams separated by 6 mrad. The vibrometer was able to accurately measure a 2500 Hz vibration target on one beam while simultaneously measuring a 700 Hz vibration target on the other.

Steering the laser vibrometer beam with the LCOS device resulted in a significant decrease in efficiency to 7.4 percent.   The efficiency loss was expected from examination of polarization states used to operate each system. Most laser radar systems operate under circular polarization in order to utilize the advantages of transmit/receive switches. Conversely, liquid crystal non-mechanical beam steering devices operate under linear polarization to ensure proper alignment with the inherent polarization.

AFIT/GSS/ENP/05-01

Acknowledgments

I would like to extend my deepest appreciation to Matthew Dierking of AFRL/SNJM for his assistance in helping me understand the physics and mechanics of the technologies used during this research. It was Matt's guidance and expertise accompanied by the additional support of the personnel of SNJM that enabled me to successfully overcome the struggles of operating various components and software applications. I would also like to separately thank Matthew Dierking and John Schmoll for the many occasions they stayed after hours or used their lunch hours to assist me in my research; for that I am indebted.

Completing a thesis in a department outside of the degree program is challenging. When the research is being preformed at a facility outside of AFIT, successful coordination of the logistics further complicate the endeavor. For managing this accomplishment, I would like to thank my advisor, LtCol Thomas Alley, for his steadfast support, his flexibility and immeasurable patience during my research.

As the world does not stop turning for academics, I would like to thank my wife for completing far more then her fair share of family and professional responsibilities while my attention was focused on research. Thank you for reconfiguring optical tables and providing a quiet study environment, while maintaining your professional and academic standards. Only with your sacrifices and support was I able to complete this milestone. I remain eternally grateful and respectful.

Kevin S. Kuciapinski

Table of Contents

List of Figures

I. Introduction

1.1 Research Motivation

The United States Air Force is focused on numerous fields of technologies designed to defend our homeland; and in that effort, to protect our war fighters. One such field of technology is the development of coherent laser radar sensing systems. Laser vibrometry lies within the sphere of laser radar sensor systems and is an effective technology for identifying and locating warfare targets.

In detecting and distinguishing targets, verification of vibration signatures is essential to accurately identify a hostile target. At present, the beam steering techniques used to collect and identify data critical to the war-fighter and decision-makers are cumbersome, mechanical systems that use motor driven mirrors or gimbaled systems. These systems are slow to react and may only collect one sample at a time. The disadvantages of the current systems are the driving factor for the Air Force's need for a laser radar steering solution.

Non-mechanical steering of the vibrometry beam would overcome these disadvantages. Liquid crystal beam steering devices are extremely light weight when compared to gimbaled systems. The phased array performance of a liquid crystal beam steering device also has the potential to simultaneously accomplish scans of multiple targets by splitting a single beam, thereby increasing the opportunity for accurate combat target identification.

1.2 Problem Statement

This thesis serves to evaluate the prospect of using a non-mechanical beam steering device to direct the beam of a laser radar system as a laser radar steering solution for future systems. The scaled experiment used for this research examines the potential of receiving accurate vibration signal returns from a laser vibrometry system (LVS) beam steered with a liquid crystal on silicon (LCOS) device; and, to explore the potential of using this non-mechanical beam steering device to split the beam of the laser vibrometer for simultaneous measurements of two independent vibration signals.

1.3 Research Objectives

1. Characterize the polarization effects induced by the LCOS device.

2. Examine the efficiency of the combined LCOS device and LVS systems.

3. Demonstrate that the laser vibrometry system may receive a vibration signal while the LVS beam is being steered by the LCOS device to 1 mrad, 2 mrad, or 3 mrad to the left or right.

4. Demonstrate that the laser vibrometry system may receive two independent vibration signals from different spatial locations while the LVS beam is being split 3 mrad to the left and right by the LCOS device.

5. Explore the viability of using a LCOS device to steer the beam of an LVS for future Air Force sensor systems by evaluation of the received signal accuracy, and the signal-to-noise ratio of the steering and sensor system combination.

1.4 Application

Current sensor system steering technologies are limited to gimbaled mirror technologies for target location, scanning, and tracking. At the same time, the present steering technologies are also limited by slow reaction times, inadequate capturing capabilities and limited data collection capacities. The ability to steer quickly is one of the LCOS device's greatest advantages. By moving quickly from one area to another a laser vibrometry system can efficiently be used to identify a combat target.

The optical phased array (OPA) used in this research is the 1024 x 768 Liquid Crystal on Silicon (LCOS) non-mechanical beam steering device manufactured by Hana Microdisplay Technologies Inc. The device is operated by supplying 255-level bitmap grayscale images to the high-resolution wavefront corrector control box. The control box then converts the grayscale images to the proper voltages for each pixel on the LCOS device to induce steering of the laser beam. This steering device will be used in conjunction with a Polytec OFV-3001 laser vibrometer. The laser vibrometer is used as a laboratory scaled experiment to test coherent laser radar steering solutions.

II. Theory

2.1 Introduction

The intention of this study is to establish whether a non-mechanical beam steering device can be used to steer the beam of a laser vibrometer. In order to grasp the challenges present in accomplishing the tasks in this study, some key background information on optics and steering light will be introduced. In addition, to gain a further understanding of the problems presented, a degree of familiarity with principal assumptions is also required. The following sections offer brief discussions of optics and light steering background, diffraction theory, liquid crystal theory, vibrometry theory and optical phased arrays (OPAs).

2.2 Optics and Light Steering Background

The Chronicles of refractive and reflective properties of optics is rich and extensive. One of the earliest known references to the rectilinear propagation of light dates back to 300 B.C.E, which was expressed by Euclid as the *Law of Reflection* in his book *Catoptrics* [3:1]. There is earlier evidence of optical technology dating back thousands of years B.C.E; but for the purpose of this thesis, the principal eras covered will be limited from the seventeenth century to present day; and the field of optical technology will be limited to diffraction and the steering of light.

2.2.1   History.   It was more than a century ago that Lord Rayleigh [John William Strutt] published an article in the *Encyclopedia Britannica* of 1888 suggesting "…that it was theoretically possible to shift energy out of the useless zeroth order into one of the higher-order spectra" [3:478]. His article stirred the attentions of a number of other physicists and scientists, who later branched off and built upon Lord Rayleigh's theory.

Among those branching scientists was Robert Williams Woods. It was 1910 that R.W. Woods built upon Lord Rayleigh's assumptions and introduced a type of grating referred to as blazed gratings. The introduction and characterization of R.W. Wood's blazed grating is significant to the advancement of light and beam steering. This research expands upon the applications of these early discoveries.

2.3 Diffraction Theory

The basic definition of diffraction is the noticeable bending and scattering of waves when they meet an obstruction. In the scientific community and applied to the characteristics of optics, Professor Francesco Grimaldi referred to the phenomenon of diffraction as "the deviation from rectilinear propagation that occurs when light advances beyond an obstruction;" something he called *"diffractio." The effect is a general characteristic of wave phenomena occurring whenever a portion of a wavefront, be it sound, a matter wave, or light, is obstructed in some way* [3:443]. For the purpose of understanding the principles of diffraction gratings used in this research the generation of secondary wavelets must be explained. The Huygens-Fresnel Principle states, "every

unobstructed point of a wavefront, at a given instant, serves as a source of spherical secondary wavelets (with the same frequency as that of the primary wave). The amplitude of the optical field at any point beyond is the superposition of all these wavelets (considering their amplitudes and relative phase) [3:444]." As the wavelets propagate, they will interfere with each other. The wavelets will either combine constructively to produce enhanced intensity or they will combine destructively canceling each other to produce nulls. The superposition of wavelets and the method for generating the super positions is of particular interest for the LCOS device operation. The LCOS device operation is based upon the principles of the diffraction grating.

The diffraction grating concepts applied in this research are based on altering the phase of the wavelets to generate the areas of constructive and destructive interference. The phase is altered by adjusting the distance that the light must travel or the optical path length (OPL). The OPL may be adjusted to either advance or retard the phase. When a wave is advanced until the path difference between two waves is equal to one wavelength of the light, the first point of constructive interference is observed. This point is known as the first diffraction order (m=1) [6]. If the wave were retarded until the path difference was one wavelength, the point of constructive interference would be the first negative diffraction order (m=-1) [6]. Similarly, a path difference of two wavelengths produces the second diffraction order (m=2), and a path difference of three wavelengths produces the third diffraction order (m=3)… It is important to mention that the specular reflection of the zero order (m=0) will always exist and methods for insuring that m=0 signals were not included in the collected data will be discussed later.

2.4 Diffraction Grating

A common method of producing diffraction orders is with the use of a diffraction grating. A diffraction grating is a group of either reflective or transmissive diffracting elements separated by a distance (*d*) determined by the wavelength of light to be diffracted [6]. The LCOS device is designed to mimic the operation of a reflective diffraction grating. A reflective grating is composed of a grating constructed over a reflective surface. For the purpose of this research, the grating modifies the phase of the electric field from the incident electromagnetic wave. Varying the distance (*d*) in a grating allows for diffraction orders m so that:

$$-2d < m\lambda < 2d \qquad\qquad (2.1) \text{ } [6]$$

The laser source in the LVS produces monochromatic light. When this light is incident upon a diffraction grating it is diffracted into discrete directions. Each groove on the grating surface is a source of diffracted light. The total light diffracted from each
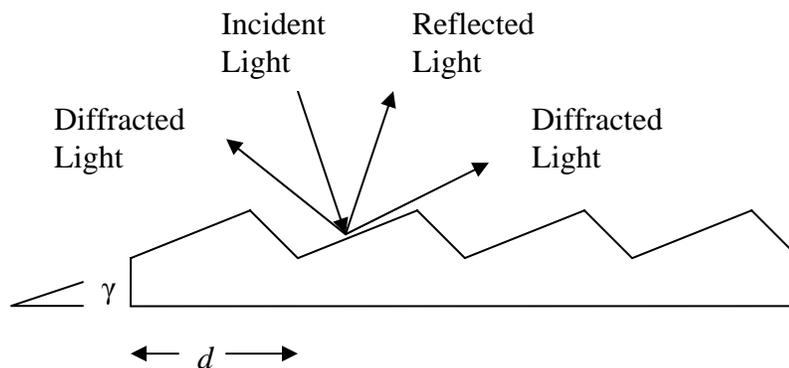
Figure 2.1: The operation of a diffraction grating [6]

groove combines to form a diffracted wavefront [6]. For a physical diffraction grating,

7

"there exists a unique set of discrete angles along which, for a given spacing d between grooves, the diffracted light from each facet is in phase with the light diffracted from any other facet, so they combine constructively" [6]. Figure 2.1 demonstrates the operation of the diffraction grating. A desired diffraction order may be generated using:

$$d \sin (-2\gamma) = m\lambda \qquad\qquad (2.2)\ [3]$$

where d is distance, γ is grating angle, m is desired diffraction order and λ is wavelength.

The endeavor to manipulate light using a non-mechanical technology involving liquid crystal on silicon (LCOS) remains subject to the tenets of the physical mechanisms used to redirect light: refraction and diffraction. However, for the technologies served by this study, steering broadband radiation with a mechanical blazed grating device is inferior to the efficient capabilities of the technologies in a liquid crystal device.

The liquid crystal on silicon (LCOS) technology examined in this study seeks to mimic the characteristics of the diffraction properties of blazed grating. Diffraction gratings are governed by the grating equation [3]:

$$d \sin \theta_m = m\lambda \qquad\qquad (2.3)$$

where θ_m is the angle to the desired order. When an incident angle is applied, such as in a blazed grating, the expression expands to [3]:

$$d(\sin \theta_m - \sin \theta_i) = m\lambda \qquad\qquad (2.4)$$

where θ_i is the incident angle of the light. The LCOS device simulates a blazed grating with an electrically generated phase ramp as shown in figure 2.2.
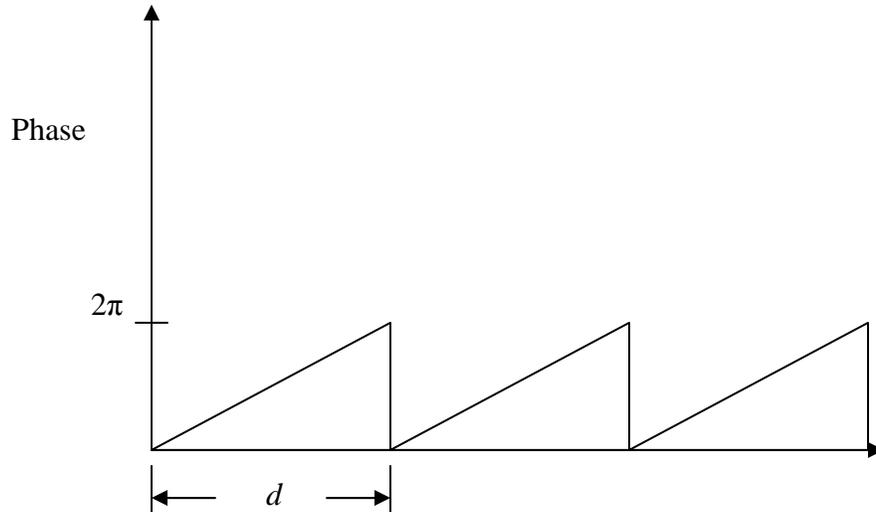
Figure 2.2: Phase ramp applied to LCOS Device

When the grating equation is applied to mathematically generate the phase ramps to operate the LCOS device, the equation is finalized as:

$$d \sin \theta = m\lambda \qquad (2.5)$$

were d is now defined as the electronic 2π phase ramp width required to produce the desired steering angle and the incident angle is zero by design of the LCOS device. This is the governing equation used to operate the non-mechanical steering device used throughout this research. The phase ramps shown above are used to assign angles to the crystals within the LCOS device. The angle of the crystal will adjust the OPL of the

wave resulting in the phase change of the electric field of the incident electromagnetic wave. The diffraction order is then realized and the beam is effectively steered.

2.5 Liquid Crystals

Duplicating behaviors of blazed gratings in the LCOS device is achieved by varying the position of the crystals and altering the optical path length of the light incident upon the device. Ensuing, the generation of a ramping effect that produces the same impressions of a physical diffraction grating. A notable added advantage to beam steering using LCOS technology is that there exists a superior variability capability inherent in the LCOS device: LCOS possesses the advantage to electronically change grating angles versus making a manual, physical change required of the mechanical blazed gratings. An additional noteworthy feature of LCOS technology is that the crystal will align itself with the applied electric field [2].

The LCOS device is an electrically controlled birefringent device [12]. That is that the liquid crystals display different indices of refraction for two different polarization axes of incident light. The thermotropic liquid crystals used in this research are a material whose rheological behavior is similar to a liquid; but, the optical response is similar to a crystalline solid [5]. This allows the crystal's orientation relative to the applied optical wave to be adjusted. The crystals orientation is adjusted when an electric field is applied to the LCOS device. The crystals change position due to both field and ionic conduction effects [5]. When applying an electric field to the crystals in the LCOS device it is necessary to oscillate the applied field to prevent a current from developing within the

10

crystal. This oscillation produced a significance effect in the results of this research that will be discussed later. When the electric field is applied to the device, the birefringence effects of the crystals are used to produce a polarization-dependent variation of the index of refraction [5]. The variation of the index of refraction generates a phase shift of the electric field within the incident optical wave. The crystals within the device may be aligned to produce the same phase effects as the diffraction grating discussed above. This is accomplished by the crystals varying their alignment along the distance of the
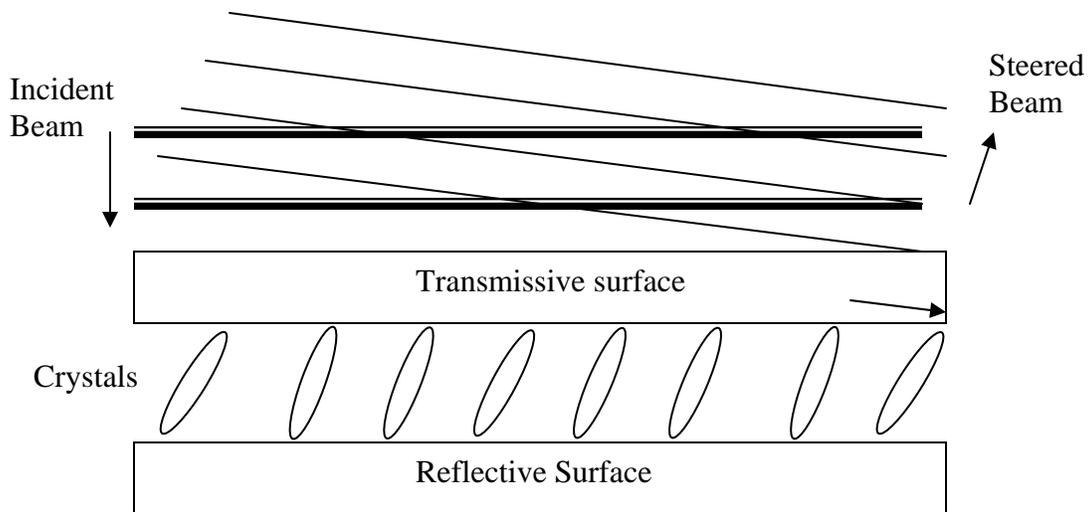
Figure 2.3: Wavefront steering by the LCOS device

phase ramp; to produce a linear change in phase of the reflected beam. Therefore, the crystals may be aligned to select a specified diffraction order, thus steering the beam. A simplified illustration of this effect is shown in Figure 2.3.

The polarization-dependant index of refraction change is critical to beam steering. In order for proper coupling of the electric field from the optical wave to the crystal, the incident optical wave must be linearly polarized and aligned with the optical axis of the

crystal. In the LCOS device, the crystals are aligned so that the optical axis is parallel to the 768 pixel axis of the 1024 x 768 device. If the incident polarization is not aligned with this axis, the emission of the steered electric field will decrease in amplitude and the orientation will be at an angle between the incident angle and the crystal axis. This point is of particular interest and will be explored for system efficiency during this research.

2.6 Vibrometry Theory

Laser vibrometry measurements are based upon the principle of the Doppler Shift [11]. A Doppler Shift occurs when a moving object either compresses or expands the waves it is generating. The phenomenon is explained well using the classic audio example of the sound from an aircraft engine. The audio example is similar to what occurs with the light's behavior in a laser vibrometer beam [8]. In this example, an airplane approaches an observer on the ground; the engine is heard by the observer at a higher frequency then the sound the engine is actually producing. This is due to the fact that the airplane is flying in the same direction that the sound waves are propagating; thus the sound waves are received at a higher frequency as shown below in figure 2.4a. When the airplane is directly over the observer on the ground, the true frequency is heard. This occurs when the aircraft movement is perpendicular to the propagation direction of the sound waves as seen below in figure 2.4b. As the airplane's relative position changes to pass directly over the observer on the ground, the engine's sound is again perceived as lower than its actual frequency production. The lowest sound heard occurs when the aircraft is traveling opposite the propagation direction causing a lower frequency than that produced by the engine such as in Figure 2.4c.
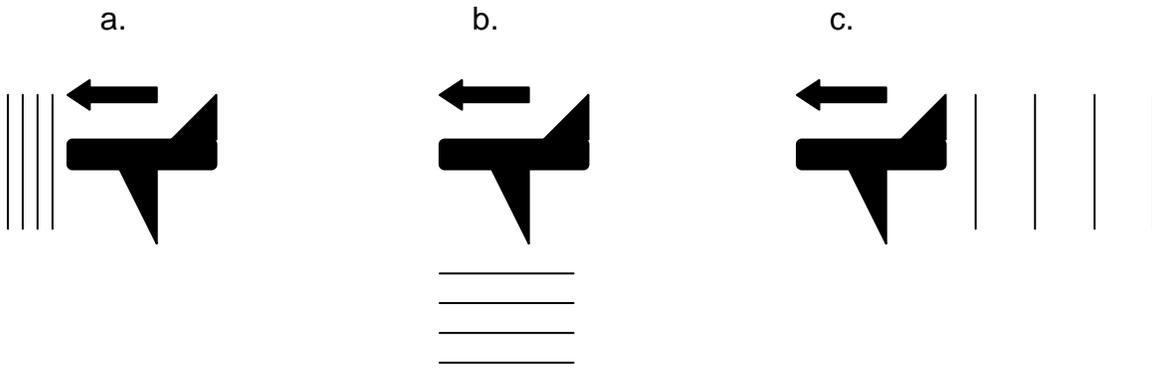
Figure 2.4 Doppler shift of sound waves illustration.

When the principles of the Doppler shift are applied to the laser vibrometer, a wave is reflected by a target and is then received by the detector inside the Laser Vibrometry System (LVS). The measured frequency shift of the wave is determined by:

$$f_D = 2v/\lambda \qquad (2.6)$$

where v is the target's velocity and λ is the wavelength of the emitted wave [11]. The Doppler shift is received by an interferometer inside the LVS where 2 coherent beams, a reference beam and the measured target beam, are combined [9]. The photo detector then measures the time dependant intensity at the point of interference by:

$$I(t) = I_R I_M R + 2K(I_R I_M R)^{1/2} \cos(2\pi f_D t + \Phi) \qquad (2.7)$$

where I_R and I_M are the intensities, respectively, of the reference and measurement beams. K is a mixing efficiency coefficient; and R is the reflectivity of the surface [11]. The phase is represented by:

$$\Phi = 2\pi\Delta L/\lambda \qquad\qquad (2.8)$$

where ΔL is the vibrational displacement of the object and λ is the wavelength of the laser light [11]. This research effort will examine if the phase changes induced by the liquid crystal steering have an effect on accuracy of the phase depended intensities at the detector of the LVS. The system configuration of the LVS is shown in figure 2.5
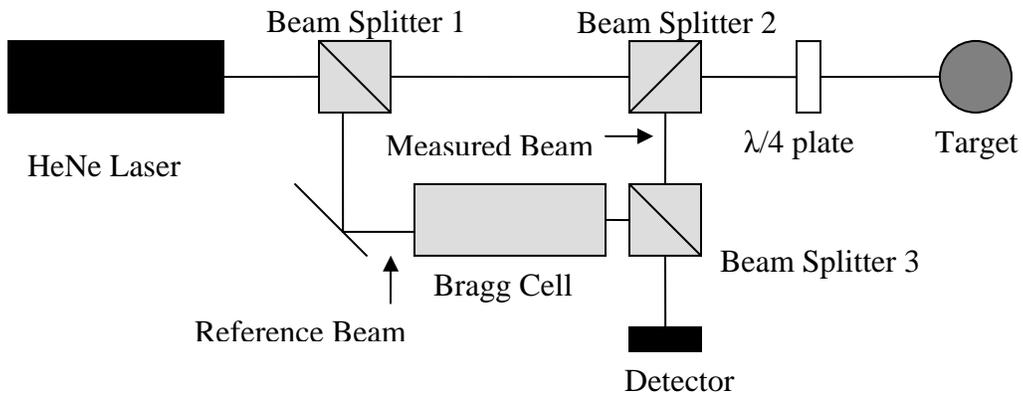
Figure 2.5: Polytec LVS

The $\lambda/4$ wave plate is used in conjunction with the polarizing beam splitter (beam splitter 2) to create a transmit/receive (TR) switch. This TR switch configuration is common for laser radar system designs and results in left circular polarization propagating to the

14

target and right circular polarization returning from the target [10]. This configuration operates under the assumption of target polarization retentiveness [4]. Beam splitter 1 separates the coherent source for the detector. Beam splitter 2 transmits the linear perpendicular laser source to the target. The $\lambda/4$ wave plate changes the linear perpendicular wave to left circular polarization. The target reflects the incident light as right circular polarization. The $\lambda/4$ wave plate then changes the returning light to linear parallel polarization. Beam splitter 2 directs the returning beam toward the detector. Beam splitter 3 combines the return beam with the source beam at the detector where the varying intensity pattern is measured. The operational configuration of the TR switch is of great interest for this research. The circular polarization of the TR switch is not compatible with the linear polarization dependence of the liquid crystals and must be investigated for effects on efficiency and accuracy of the LVS.
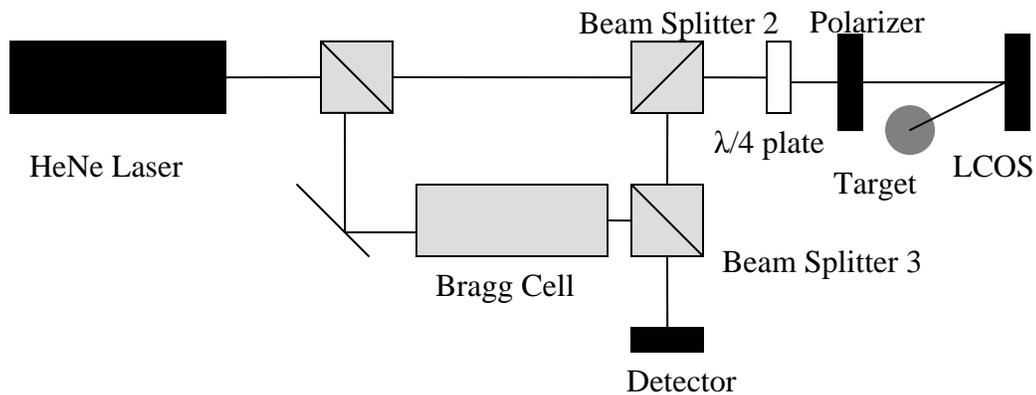
Figure 2.6: Combined Configuration

The goal of this study is to produce a successful vibration measurement while the laser radar beam is steered by the LCOS device. The final configuration combining both systems is shown in figure 2.6.

III. Methodology

3.1 Introduction

By applying the theory discussed in chapter 2 it is possible to combine the independent technologies of the Liquid Crystal on Silicon (LCOS) non-mechanical steering device and the Polytech Laser Vibrometer System (LVS). This research begins with independent analysis of each system's characteristics, then proceeds to the proof of concept demonstration using the LCOS device to steer the beam of the LVS.

3.2 LCOS Operation

The HANA LCOS non-mechanical beam steering device is operated by supplying a specific grayscale phase steering image generated for each desired steering angle. The induced phase shift is controlled by varying the width, or number of pixels contained within each phase ramp. The number of pixels required for a ramp is calculated by finding the ramp width using the equation:

$$d = \lambda/\sin\theta \qquad (3.1)$$

where *d is the* ramp width, λ is the wavelength, and θ is the steering angle.

The width of each pixel on the HANA LCOS device is 20µm. Therefore, the number of pixels in each ramp is calculated from the ramp width and pixel width using the equation:

$$\rho = d/\mathrm{x} \qquad\qquad (3.2)$$

where ρ is the number of pixels, *d* is the ramp width, and x is the pixel width.

Applying the equations listed above, grayscale phase steering images were calculated for angles of 0mrad, 1mrad, 2mrad, and 3mrad in both the left and right directions which are shown in figures 3.1-3.7. The MATLAB code used to generate the steering images is located in Appendix A.

The phase ramps used to produce steering assume that the surface of the LCOS device is completely flat. However, non-uniform curing of the adhesives in the manufacturing process cause the surface of the LCOS to become curved [12]. The slope of the surface of the device induces additional phase changes. To correct for these errors a phase compensation image (figure 3.1) was provided by Kent State University [12]. This compensation image is used to create a grayscale phase image that generates a flat surface profile of the liquid crystals. The phase ramps used for steering are combined with this image to produce the desired steering angles.
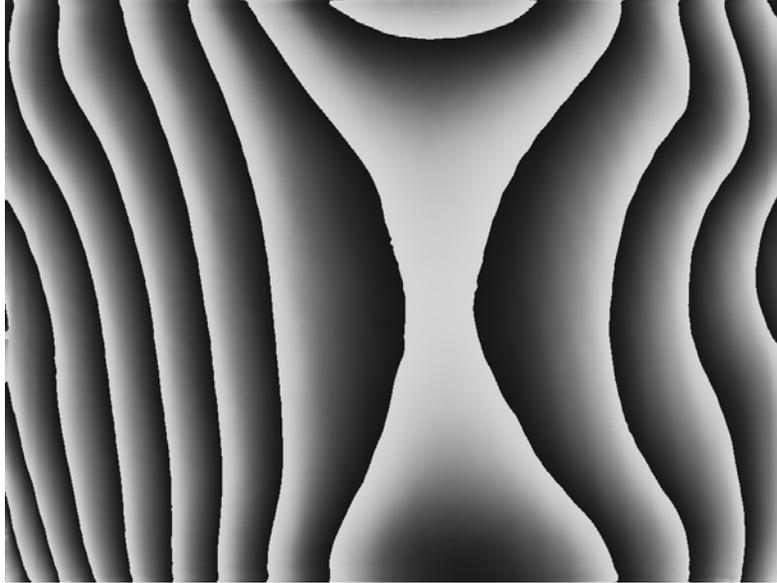
Figure 3.1: Compensation image used to adjust for surface distortions in the LCOS device, also representative of a 0 mrad phase ramp
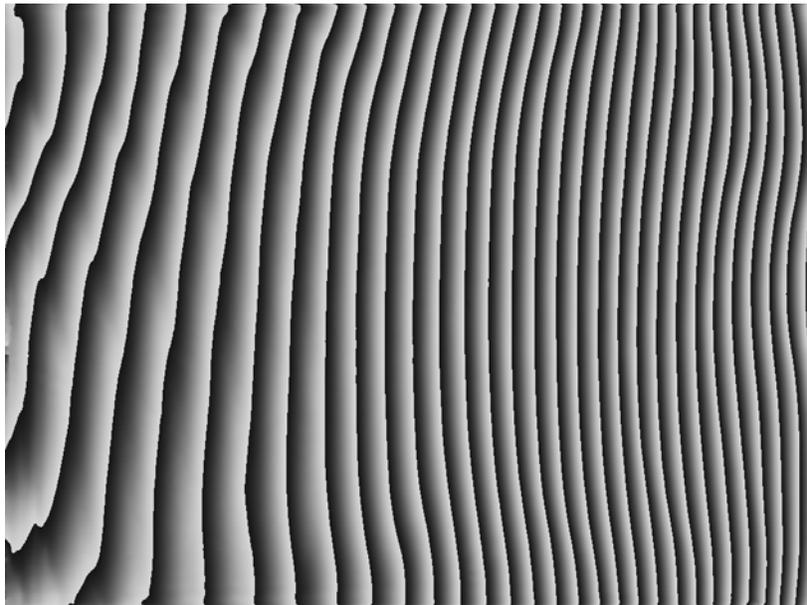
Figure 3.2: Phase steering image for 1 mrad left
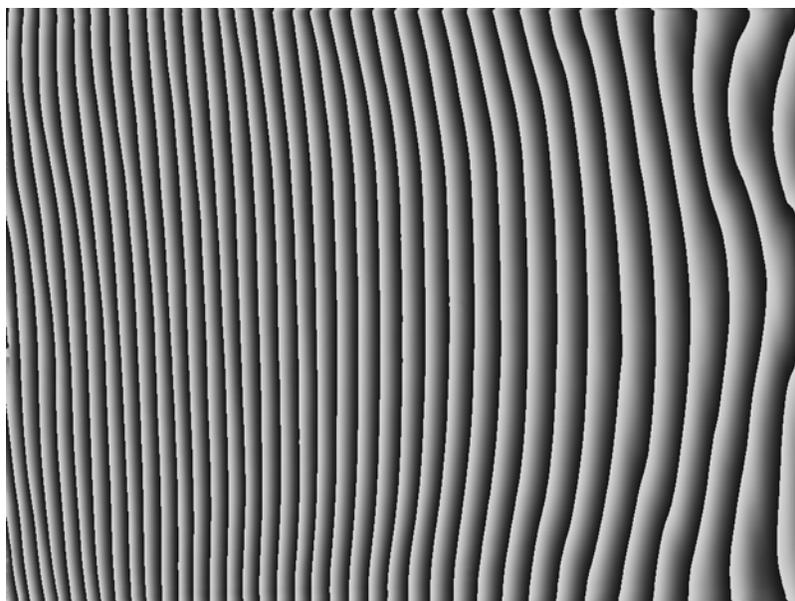
Figure 3.3: Phase steering image for 1 mrad right
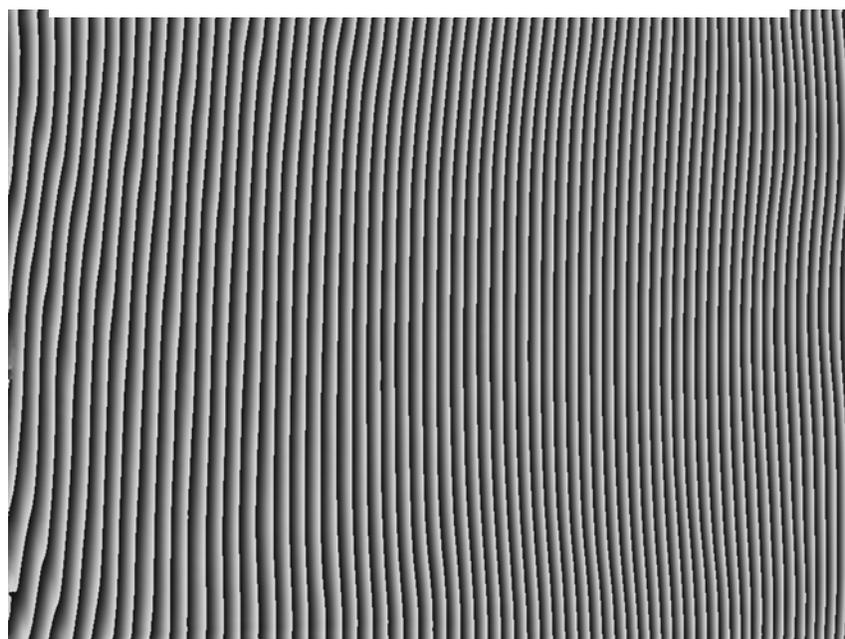
Figure 3.4: Phase steering image for 2 mrad left
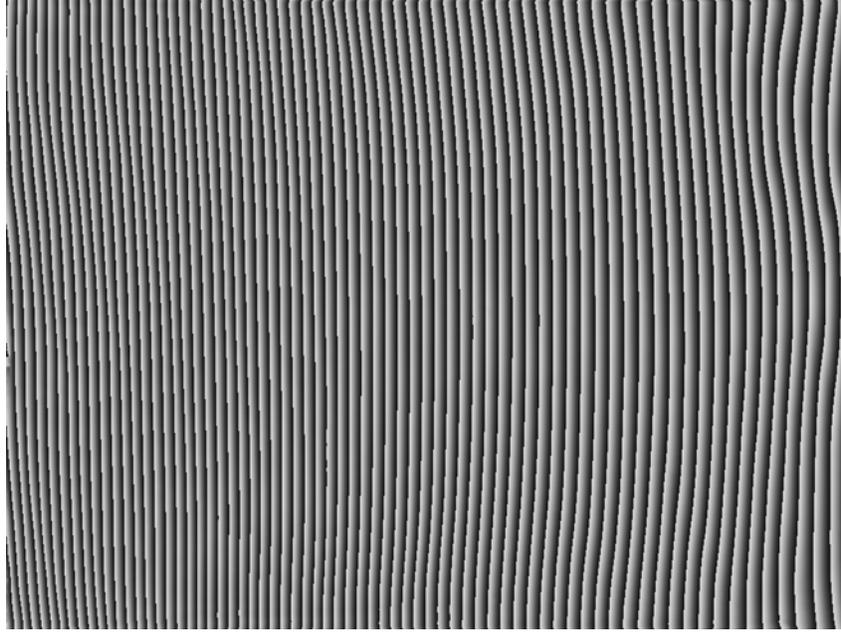
Figure 3.5: Phase steering image for 2 mrad right
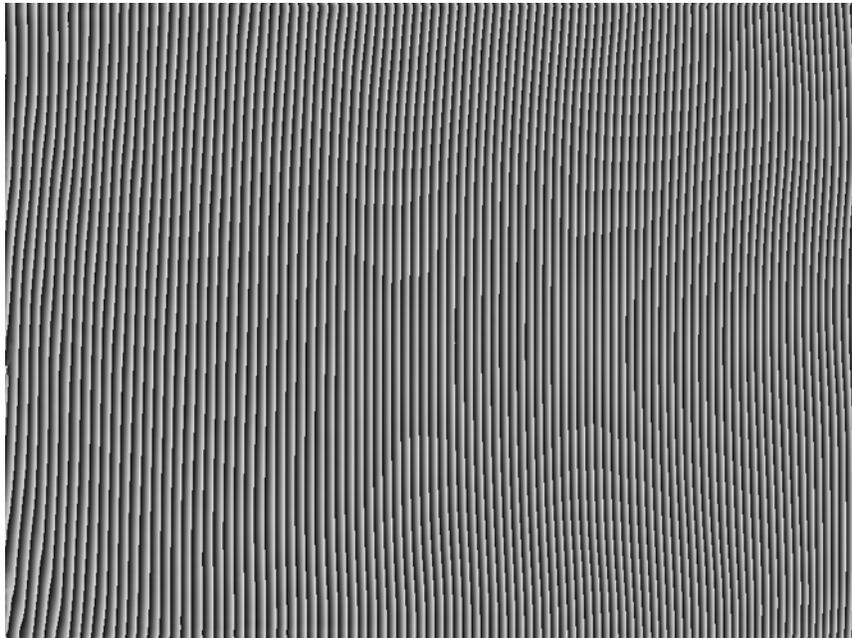
Figure 3.6: Phase steering image for 3 mrad left
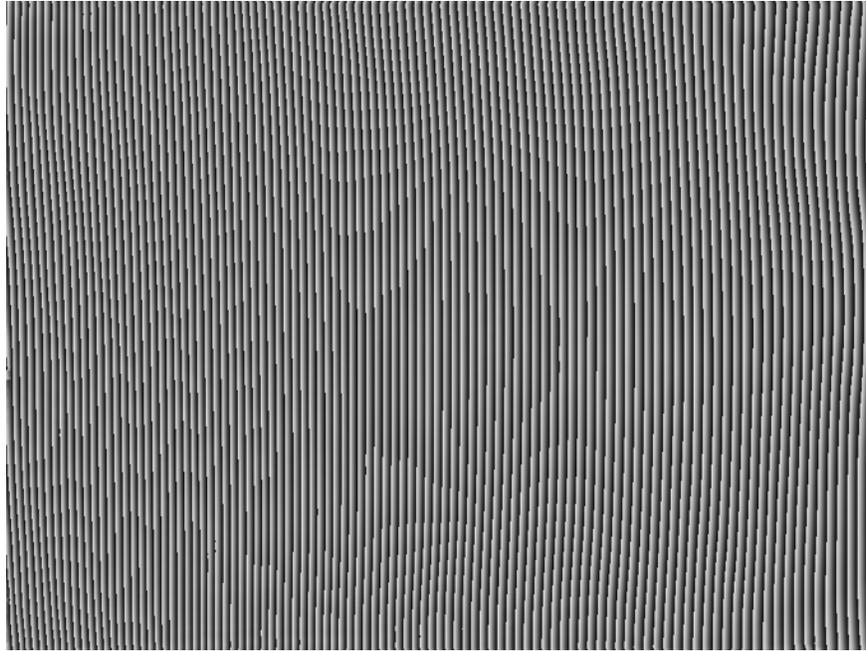
Figure 3.7: Phase steering image for 3 mrad right

3.3 Polarization Effects

Polarization state is essential to ensure accurate steering and maximum efficiency of the LCOS device. Appropriate operation of the LCOS device requires that the incident light is polarized along the fast axis, or optical axis of the apparatus. The orientation of the LCOS device used in all experimental set-ups during this research effort required the light incident upon the device to be in the linear vertical polarization state.

Once the incident light supplied to the LCOS device was in the proper polarization state, it was necessary to measure changes to the polarization state induced by the steering of the device. Polarization changes induced by the device give rise to a possible reduction of efficiencies; and at the same time, could also generate compatibility challenges between the LCOS device and the Polytec LVS. The experimental set-up

21

shown in figure 3.8 was used to measure the polarization changes induced by the LCOS

steering of the incident light. A 5mW HeNe laser with a polarizer was used to provide

incident light at the proper orientation. The intensity of the steered beam was then

measured with a power meter after it passed through a second polarizer. The second

polarizer was rotated to find the peak intensity of the steered beam. The angular

difference between the first and second polarizer represented the rotation of polarization

caused by the LCOS device.
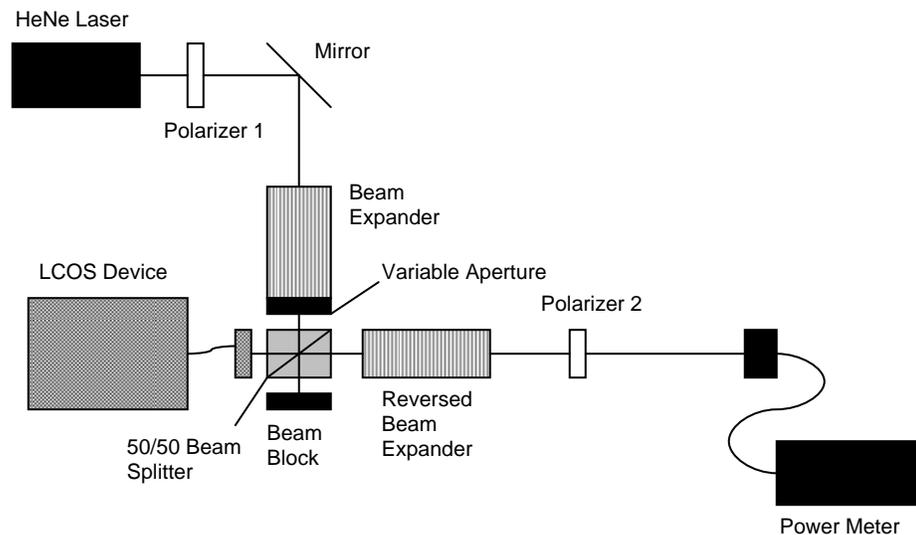
Figure 3.8: Configuration for single pass polarization measurements

When the LCOS device steers the beam of the Polytech LVS, the light first travels

through the LCOS device then reflects off of the target and travels back through the

LCOS device a second time, returning to the LVS. Therefore, after the initial

polarization changes induced by the LCOS device where measured, it was necessary to

examine the polarization effects following a second pass through the device. Simply

reflecting the steered beam back through the LCOS device in figure 3.8 resulted in low-

level intensity that produced inadequate concentrations for measure. As a consequence, second pass polarization measurements where accomplished using a pair of HeNe lasers as shown in figure 3.9. The beam of the first laser was steered to the desired angle. The second laser, providing a 5mW beam in the opposite direction was then placed directly at the spot of the steered order from the first laser. At this time the first HeNe was turned off and all reverse measurements were taken from the second HeNe.

Using the results from the single pass polarization experiment, polarizer 1 was set at the angle which the polarization was rotated to form the single pass through the LCOS device. Accordingly, the second HeNe then simulated reflection from the target at the induced polarization state after beam steering. The intensity of the steered beam was again measured with a power meter after it passed through the second polarizer. The second polarizer was rotated to find the peak intensity of the simulated return beam. The angle of peak intensity on the second polarizer then represents the polarization state after the beam passes through the LCOS device in both directions as illustrated in figure 3.9.

Figure 3.9: Configuration for second pass polarization measurements

3.4 Efficiency

A successful proof of concept demonstration on the use of a non-mechanical steering device to steer the beam of a laser vibrometer demands as a minimum, that the combined system be efficient enough to receive a signal along the reflected steered beam. The requirement of a second HeNe laser to provide a simulated return signal demonstrated that the previous experimental set-up was too inefficient to provide an adequate return intensity to the laser vibrometer. By design, The HANA LCOS device steers most accurately and efficiently when the incident angle is normal to the steering device. In order to reach an adequate level of overall combined efficiency between the LCOS and the LVS, a small incident angle (5.71 degrees) upon the LCOS device was required during reconfiguration as shown in figure 3.10.
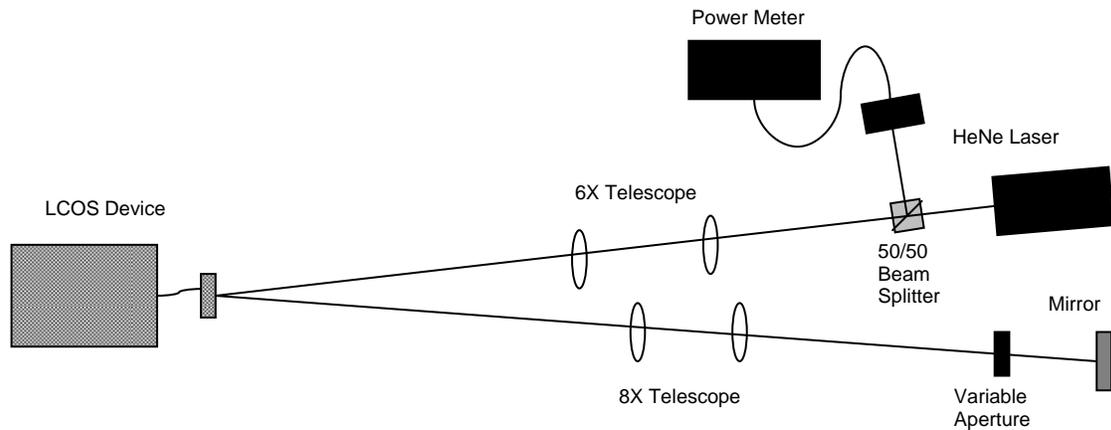
Figure 3.10: Configuration for efficiency measurements

24

A 6X telescope was required to ensure that the spot size of the HeNe laser at the LCOS device encompassed all available pixels on the surface of the device. For measurement and experimentation purposes, the 8X telescope was necessary to ensure that the steered orders could be adequately separated from surrounding orders. The variable aperture was used to remove the unwanted orders from the system. The short propagation distances on the optical table caused the diffraction orders to be very close to each other, necessitating the variable aperture. Although maximum efficiency of all components would have been ideal, trade-offs were made between components in order to achieve the goal of completing a successful combined system proof of concept demonstration for this research effort.

3.5 Vibration Measurements

The overall goal of this research effort was to prove that a laser vibrometer beam could be directed with the use of a non-mechanical beam steering device. Therefore, once a sufficient level of efficiency between the systems could be achieved, it was necessary to examine whether a vibration signal could be received through the Polytech LVS beam steered by the LCOS device; and whether the received signal was accurate. This experiment was conducted by replacing the HeNe laser with the Polytech LVS as shown in figure 3.11.
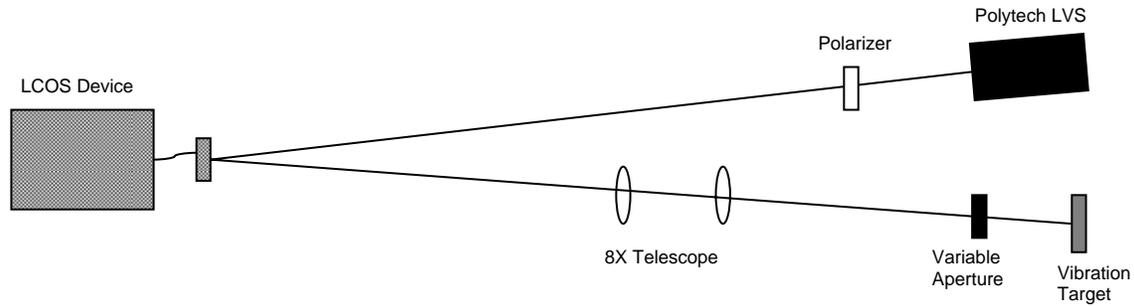
Figure 3.11: Configuration for vibration measurements

In this set-up, the polarizer was used to ensure that the beam from the LVS was incident upon the LCOS device at the proper polarization. The 8X telescope was used to create separation between the diffraction orders after steering of the beam while the variable aperture blocked all but the desired order. A frequency generation box was used as the vibration target. Therefore, the frequency and amplitude of the target could be adjusted. Additionally, the target frequency received by the Polytech LVS could be compared to the known frequency of the source. The objective was to receive an accurate signal for the target at each steering angle.

While accurate reception of the vibration signal was a primary aim in this study, it was also necessary to ensure that the received signal was discernible above any noise induced by the device. To properly capture all data related to LCOS induced noise, the vibration target was replaced with a mirror and a noise frequency power spectrum was captured for each steering angle.

3.6 Split Beam Vibration Measurements

To effectively use laser vibration measurements as a tool for combat target identification and location requires a responsive steering solution. Current gimbaled technologies require the motor to swing the beam from point to point to capture target measurements. The advantages of an OPA serve to overcome this limitation. The quickest way to accomplish several scans is to split the beam from the sensor and simultaneously capture multiple vibration waveforms. To simulate this scenario in the laboratory and test the concept of splitting the LVS beam with the LCOS to receive two independent vibration waveforms, the configuration in figure 3.12 was used.
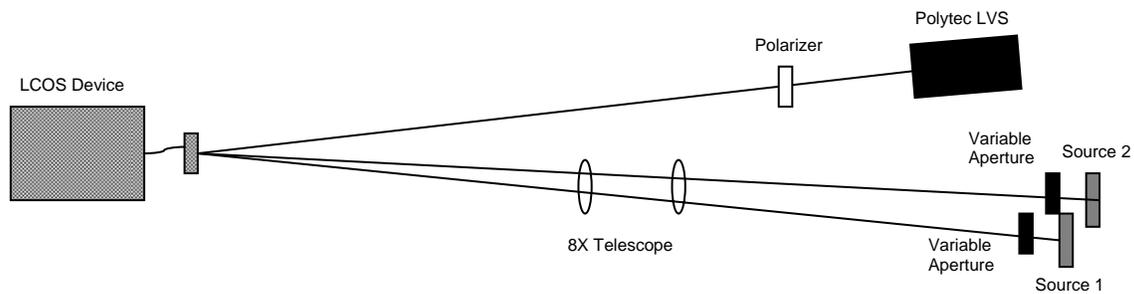
Figure 3.12: Configuration for split beam vibration measurements

In this configuration the single beam leaving the Polytech LVS is split equally into 2 individual beams separated by 6mrad. The frequency generation box was used as the source for one beam while a tuning fork was used as the source for the other. Once

again, the telescope provided adequate separation of diffraction orders and the variable

apertures eliminated the undesired orders.

3.7 Summary

This section addressed the experimental configurations used to accomplish the

research objectives and operation of the systems. The successful combination of the

LCOS non-mechanical beam steering device and the Polytech LVS require special

attention in the areas of polarization state and overall combined efficiency. With the

proper configuration between the two systems, great potential is demonstrated that

supports the use of a non-mechanical beam steering device to accurately direct the beam

of a laser vibrometer. The next section will address results of the effort to combine the

two technologies.

IV. Results and Analysis

4.1 Introduction

Laser vibrometry measurements are accomplished using the system described in section 3.5. The laser vibrometry system beam was steered and split using the LCOS device described in section 3.2. The following chapter will present detailed results and descriptions of analysis collected during research.

4.2 Test Cases

The theory and operation of the LCOS and the LVS identified several possible conflicts for the integration of the two technologies. The goal was to illustrate the possibilities of using a non-mechanical beam steering device to control the beam of a laser vibrometry system for combat target identification and location. The following is a list of the criteria:

- Determine the polarization effects induced by the LCOS device

- Measure the efficiency of the LCOS and LVS combination

- Steer the LVS with the LCOS device to track a vibration target signal

- Explore signal detection capability of the LVS signal transmitting through the LCOS against the noise produced by the LCOS device

- Split the LVS beam with the LCOS device to detect 2 separate vibration target signals

4.3 Polarization Effects

The polarization of the LVS beam is important to the efficiencies of: a) the return signal within the LVS; and, b) the beam's passage through the LCOS device. The polarization of the beam returning to the LVS is a critical function as it ensures that the signal returning from the target is directed to the internal detector of the LVS. The polarizing beam splitter located at the aperture of the Polytech LVS transmits light which is polarized linear perpendicular and reflects light of the polarization linear parallel [7]. As shown in figure 2.5, between the polarizing beam splitter and the vibrometer aperture there is a $\lambda/4$ plate. This combination results in linear perpendicular polarization leaving the laser, transmitting through the polarizing beam splitter, the $\lambda/4$ plate then converts the polarization linear perpendicular to circular polarized light propagation to the target. The circular polarization is then reflected from the target passing back through the $\lambda/4$ plate which converts the polarization to linear parallel. The linear parallel polarization is then reflected to the LVS detector by the polarizing beam splitter.

Conversely, the LCOS device requires linear polarization along the fast axis of the device for proper operation and maximum steering efficiency. This presents a system configuration challenge when integrating the LCOS device with the LVS. To accomplish the integration, a linear polarizer was placed immediately after the LVS aperture to properly orient the polarization for the LCOS (figure 2.6). This resulted in an efficiency loss of 50 percent.

In order to fully examine the polarization effects induced by the LCOS device, measurements were captured after a one-time pass of the HeNe laser through the LCOS;

as the laser was reflected and returned for a second pass through the LCOS another measurement was captured and recorded.

The single pass measurements were accomplished using the set-up shown in figure 3.8. It was found that the LCOS device created a 5 to 12 degrees rotation in the linear polarization when the HeNe beam passed through it. As the device steered to greater angles of deflection, the amount of polarization rotation was discovered to increase. Furthermore, the results indicate that polarization rotation increases at a greater rate when steering to the right versus the left. The signal pass polarization results are shown in figure 4.1 for steering to the left and 4.2 for steering to the right.
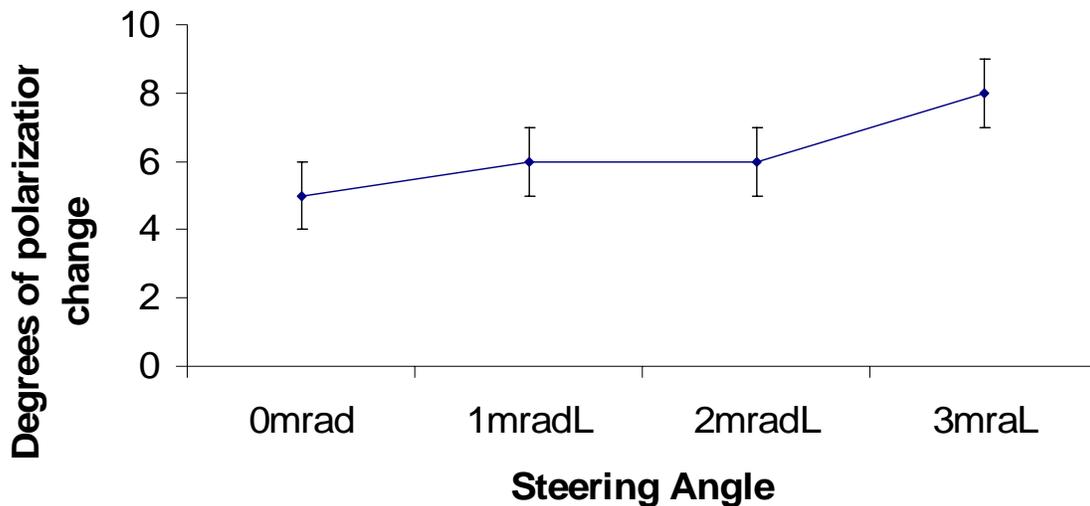
Figure 4.1: Single pass polarization rotation induced by steering left
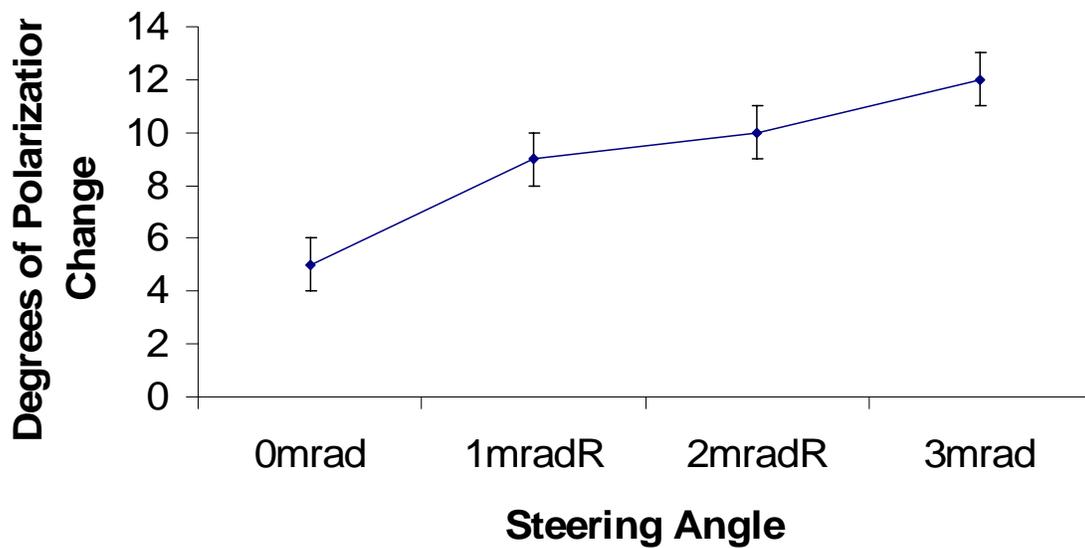
Figure 4.2: Single pass polarization rotation induced by steering right

The double pass polarization measurements were accomplished using the set-up shown in figure 3.9. This experiment found that the second pass of the HeNe beam through the LCOS corrected a majority of the polarization rotation induced by the initial pass of the beam through the device. The net polarization rotation from both passes was determined to increase with steering angle when the beam was steered to the right as shown in figure 4.3.
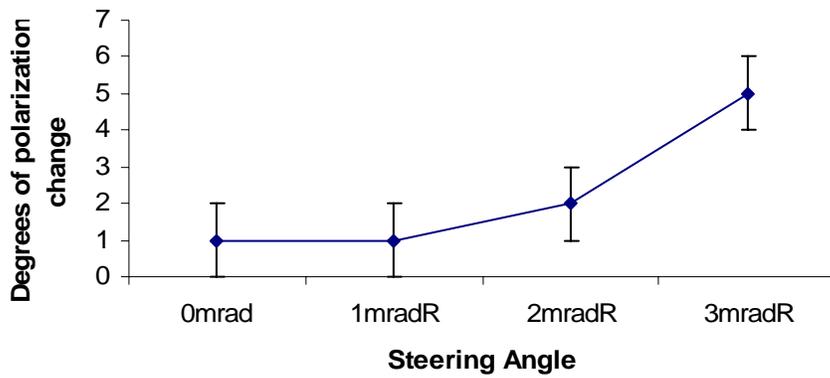
Figure 4.3: Double pass polarization rotation induced by steering right

When the LCOS steered the beam to the left the net polarization rotation did not show an increase with steering angle. Instead, the net polarization rotation from both passes appeared to remain within a half degree of 1.5 degrees as shown in figure 4.4.
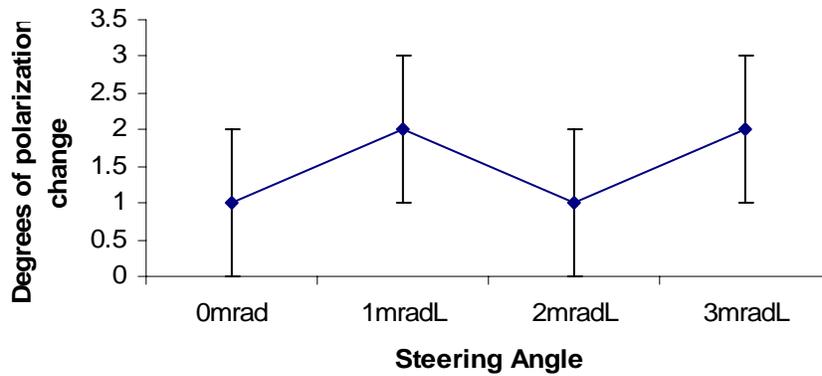
Figure 4.4: Double pass polarization rotation induced by steering left

4.4 LCOS and LVS combined efficiencies

The LCOS device is designed to operate with an incident beam oriented at the normal, which gives it a maximum efficiency of 77.2 percent [12]. However, the configuration used to achieve the normal incident angle resulted in an undetectable return intensity. A detailed link budget analysis of the combined optics in figure 3.8 showed that only 0.2% of the original intensity from the first laser was returned before the device was used for steering. Thus, the use of a second laser was required to provide a level of intensity to accomplish the polarization measurements (figure 3.9).

For combined system operations, the decision to use a slight incident angle as shown in figure 3.10 was determined to be the most advantageous for mitigating signal loss. Even with the efficiency losses induced by the angle, it was possible to receive a return signal and measure the efficiency of the combined LVS and LCOS device system. The system efficiency was calculated using the equation:

$$e = r/i \qquad\qquad (4.1)$$

where e is the efficiency, r is the return intensity, and i is the incident intensity.

Beginning with a 5 mW HeNe laser the reflected non-steered beam was measured at 185 µW resulting in a combined system efficiency of 3.7% with a 50/50 beam splitter in place for a power meter (figure 3.10). Mathematically adjusting for the beam splitter shows a 2.5 mW beam is incident upon the LCOS device; and a 370 µW beam is returning from the LCOS device with the power meter beam splitter removed. At the

conclusion of the double pass process through the LCOS device, the aforementioned calculations provide 14.8% efficiency.

To calculate the efficiency values of the complete LVS and LCOS device combination, the previous return values of the 5 mW source and the 370 µW LCOS device were used. The 370 µW return value is used for this calculation because it was generated from the 5 mW source with the 50/50 beam splitter measurement. The beam splitter reduced the 5 mW intensity to 2.5 mW. This is the same 50% loss expected from the polarizer used with the LVS. Therefore, the combined LVS and LCOS device effectiveness is calculated as 7.4% efficiency.

There are several factors depleting intensity from the combined system. As discussed in the previous section, independently, the LCOS and the LVS are designed to operate in non-compatible polarization states. By forcing the LVS into the same linear polarization state used by the LCOS device, the initial beam immediately encountered a 50% reduction of intensity.

The second dominate intensity loss is that the HANA LCOS published maximum efficiency of 77.2% was never realized. As calculated above, the double pass efficiency was found to be lower than anticipated with 14.8% efficiency. In addition to the losses generated by introducing an incident beam angle, research performed by Kent State University using the HANA LCOS device highlighted another loss: Kent State researchers discovered that the device does not maintain its physical shape while operating [12]. As the physical shape fluctuates with temperature changes during operation, the precision of the generated grayscale steering images is compromised. This creates a steering deficiency. Further contributing to these losses is that the LCOS device

mounting surface was changed prior to this research effort. The surface compensation

image discussed in Section 3.2 and shown in figure 3.1 is used to adjust for the LCOS

device not being perfectly flat. The compensation image used to correct for the physical

surface errors is generated after the LCOS device is mounted. Changing the mounting

surface at a later date degrades effectiveness of the compensation image further

decreasing the steering efficiency. Generating a new compensation image would correct

this discrepancy. However, due to time constraints the steering efficiency was deemed

acceptable to continue with the research objectives.

Although the 7.4% measured efficiency of the combined systems is low, it was

suitable to complete a successful proof of concept demonstration. The goal of this

research was to successfully receive a steered vibration target signal, which was made

possible by accepting the configuration generated losses within the system.

4.5 Steering to a Vibration Signal

Using the generated steering images discussed in Chapter III, the beam of the

LVS was steered in both the left and right direction to angles of 1mrad, 2mrad, and

3mrad. After the LVS was steered, all undesired diffraction orders were removed from

the target area with a variable aperture to prevent added signal returns from any

diffraction orders outside of the steered order. A 2500Hz vibration signal was then

applied to the steered order with the frequency generator box. In each case, the

appropriate signal waveform was properly measured by the LVS. For each waveform

measurement, 4096 data points were collected. To display the amount of power located

within each frequency of the received waveform, a Fourier Transform was preformed.

The Fourier Transform produced the frequency power spectrums used for analysis of the

vibrometer results. The frequency power spectrums of each waveform show the target

signal several orders of magnitude above the system noise.   Figures 4.5 through 4.10

show the 2500Hz signal at each of the steering angles.
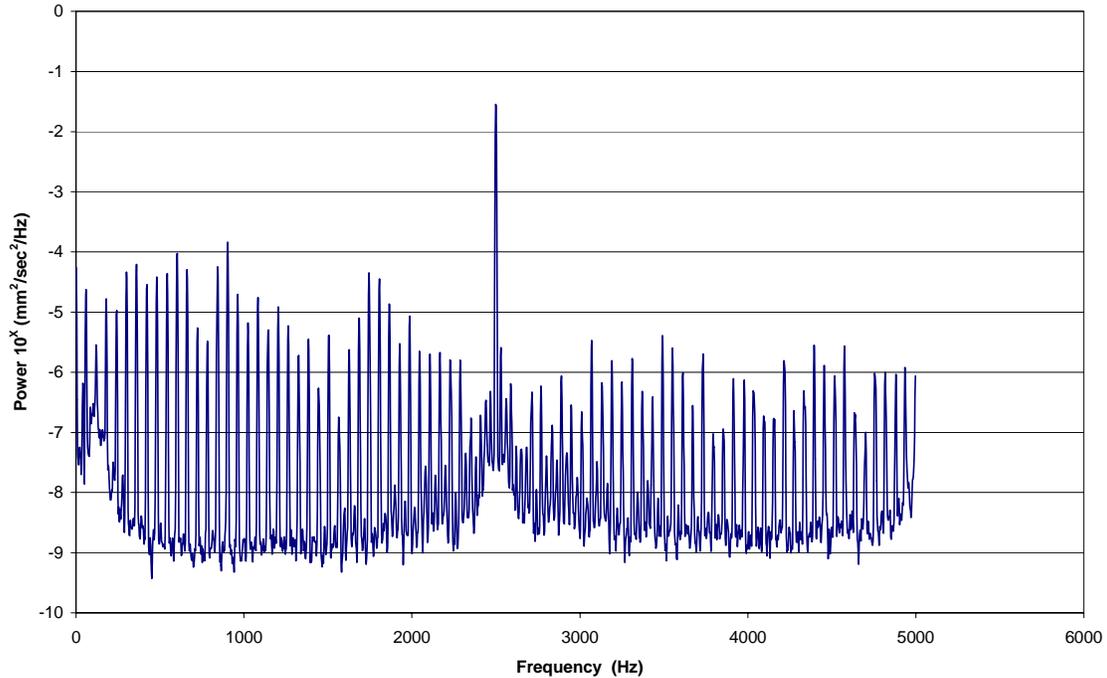
Figure 4.5: 1mrad Left Average Power Spectrum: LVS tracking a 2500Hz target
while being steered 1mrad to the left by the LCOS device.
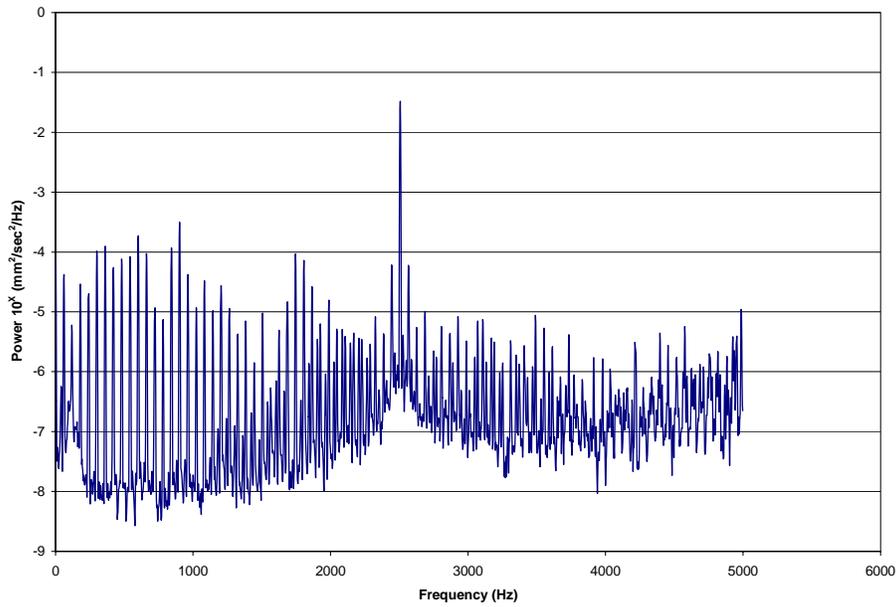
Figure 4.6: 1mrad Right Average Power Spectrum: LVS tracking a 2500Hz target while being steered 1mrad to the right by the LCOS device.
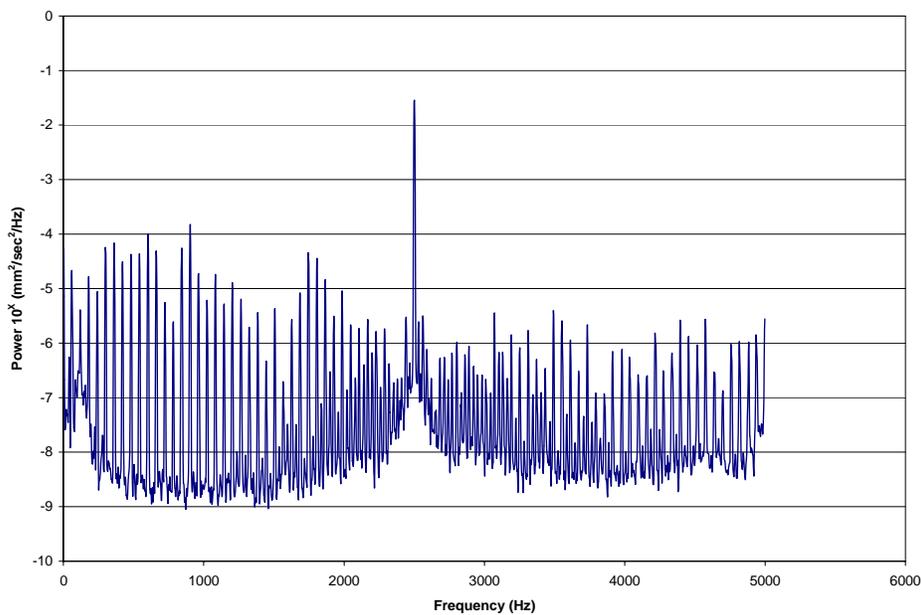
Figure 4.7: 2mrad Left Average Power Spectrum: LVS tracking a 2500Hz target while being steered 2mrad to the left by the LCOS device.
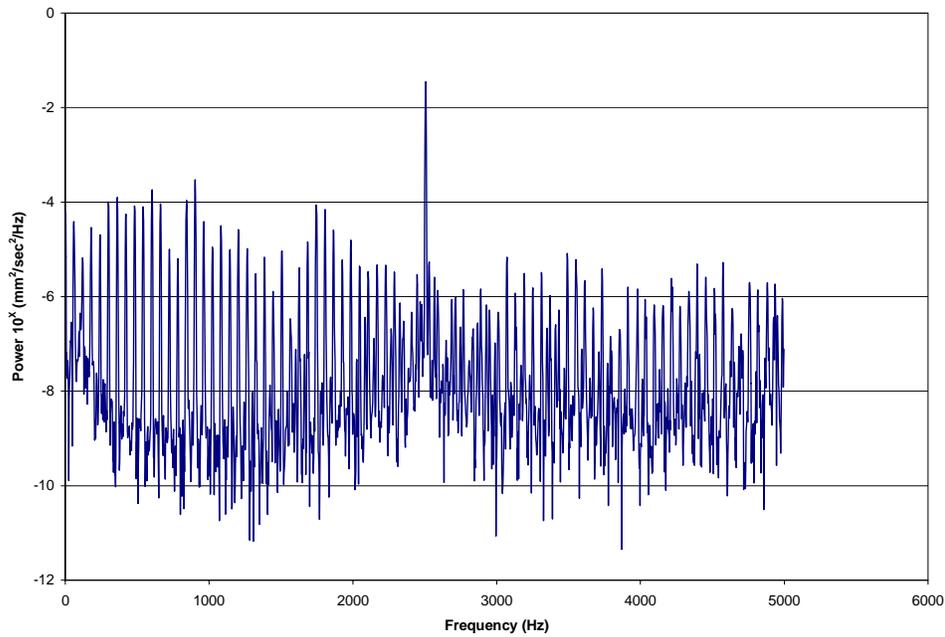
Figure 4.8: 2mrad Right Average Power Spectrum: LVS tracking a 2500Hz target while being steered 2mrad to the right by the LCOS device.
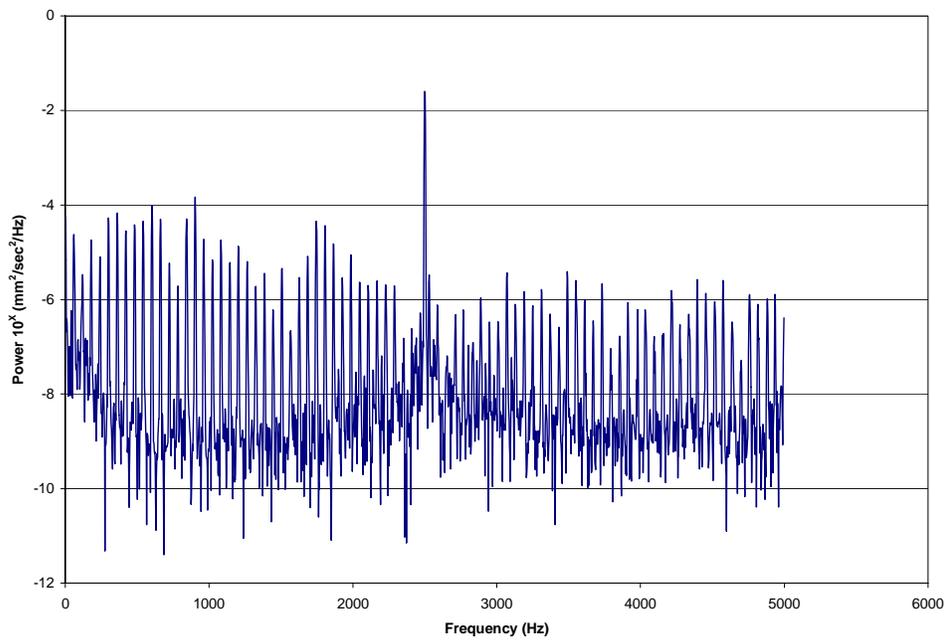

Figure 4.9: 3mrad Left Average Power Spectrum: LVS tracking a 2500Hz target while being steered 3mrad to the left by the LCOS device.
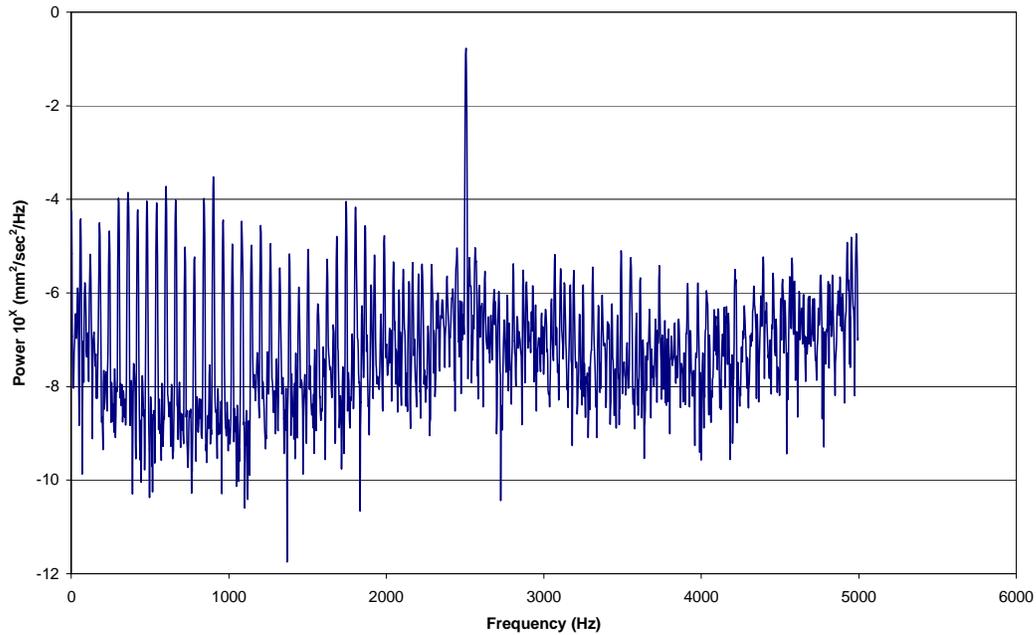
Figure 4.10: 3mrad Right Average Power Spectrum: LVS tracking a 2500Hz target while being steered 3mrad to the right by the LCOS device.

Comparing the signal received across steering angles showed that the signal strength remained relatively unaffected by the steering angle. The actual data is shown in figure 4.11. In this figure the signal intensity appears to increase when the beam is steered to 3 mrad right. After further investigation an experimental error was found. The 3 mrad right data point was sent a vibration signal at twice the intensity of the other measurements. An adjustment was made to the data by decreasing the signal intensity by half at the 3 mrad right data point. The adjusted results in figure 4.12 demonstrate consistent signal intensity across steering angles.
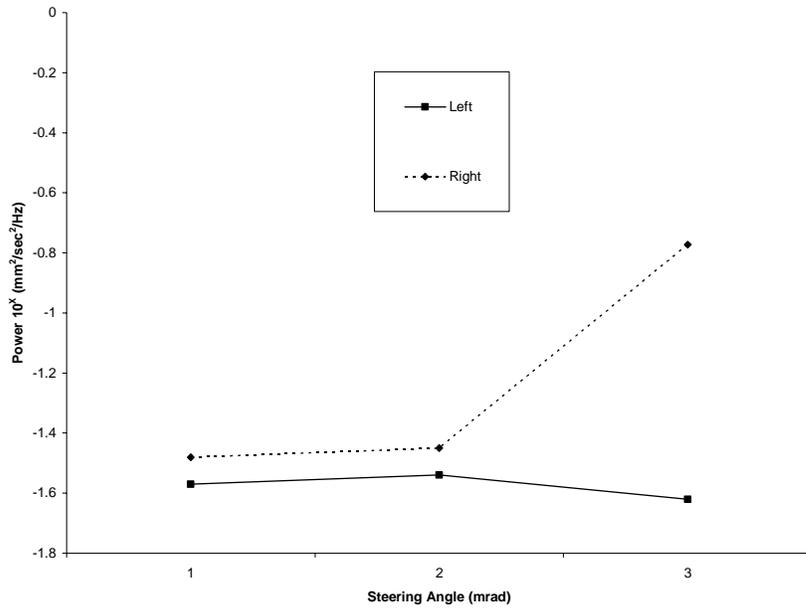
Figure 4.11: Signal Intensity vs. Steering Angle
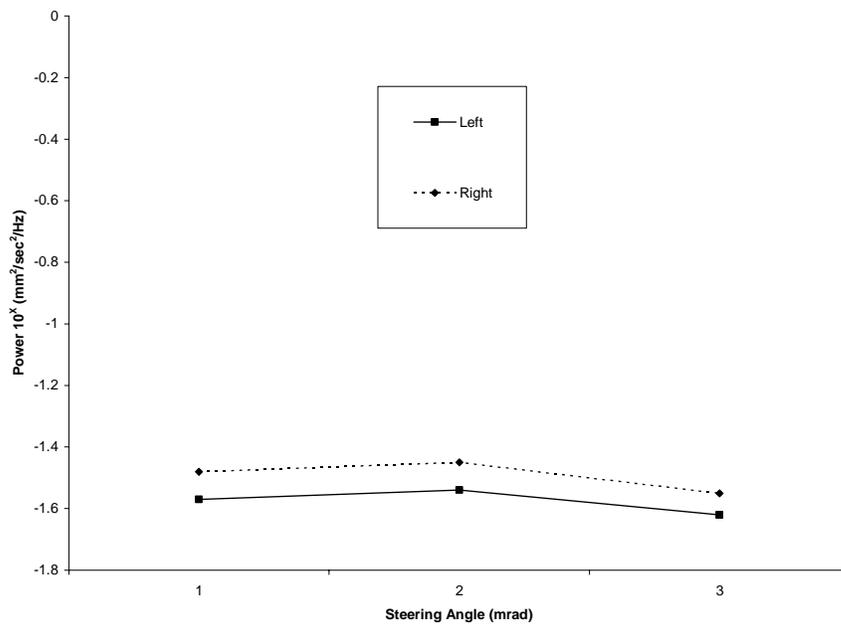
Figure 4.12: Adjusted Signal Intensity vs. Steering Angle

4.6 Steering the Laser Vibrometer without Target

During the vibration measurements, a small noise signal was observed to have been generated by the LCOS device as shown on the logarithmic scale in figure 4.13.
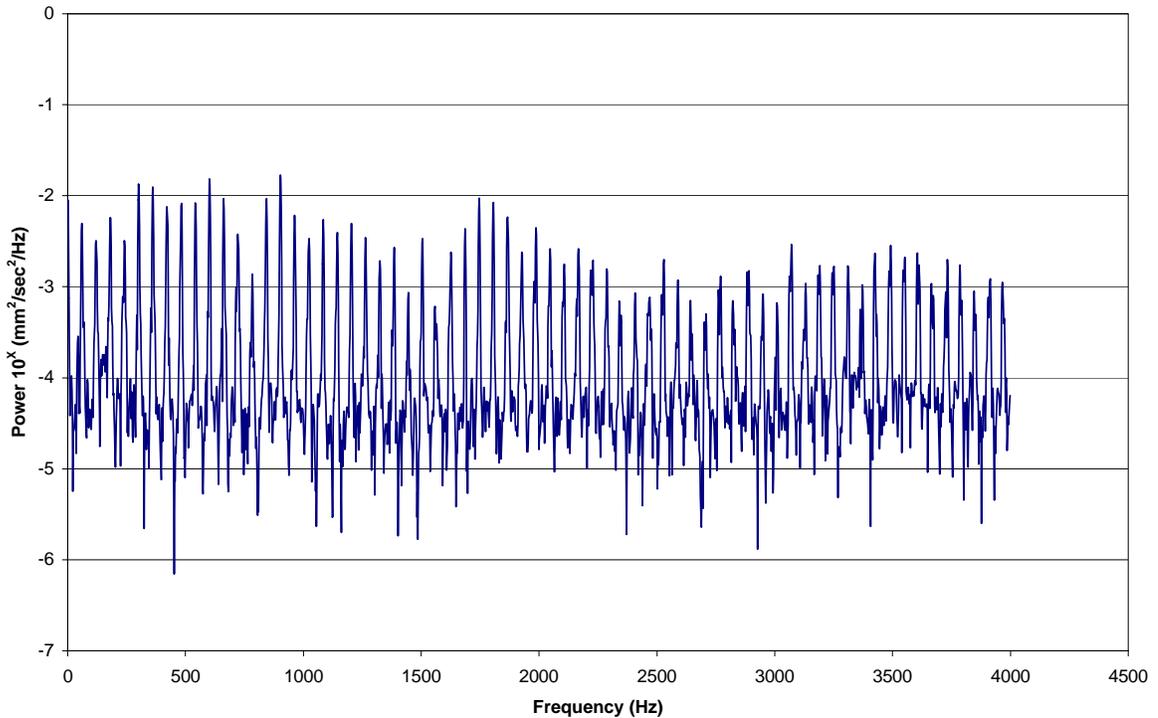
Figure 4.13: LCOS Device Induced Noise on Log Scale: Power spectrum of noise induced when compensation grayscale image is applied.

After testing to ensure that the experiment was vibration isolated, the LCOS device was determined to be the source of the noise. The optical table was floated and dampened. With the exception of the LCOS device control box, all operating electrical equipment was removed. To ensure that the control box and LCOS device were not

vibrating, the LVS was focused on the control box and then the LCOS device mount. No vibration or noise signal was visible in either case.

　　With external noise ruled out, steering images were applied to the combined LVS and LCOS device system as in section 4.5 without a target vibration signal. The noise induced by the device was found to be consistent regardless of the steering command applied to the device. The noise diminished only when the control box for the LCOS device was powered off as shown in figure 4.14. The only other decrease in the noise was observed in figure 4.15 when the LCOS device was on with an all zero array, or black screen was applied. This plot is shown in a linear scale to highlight key noise frequencies.
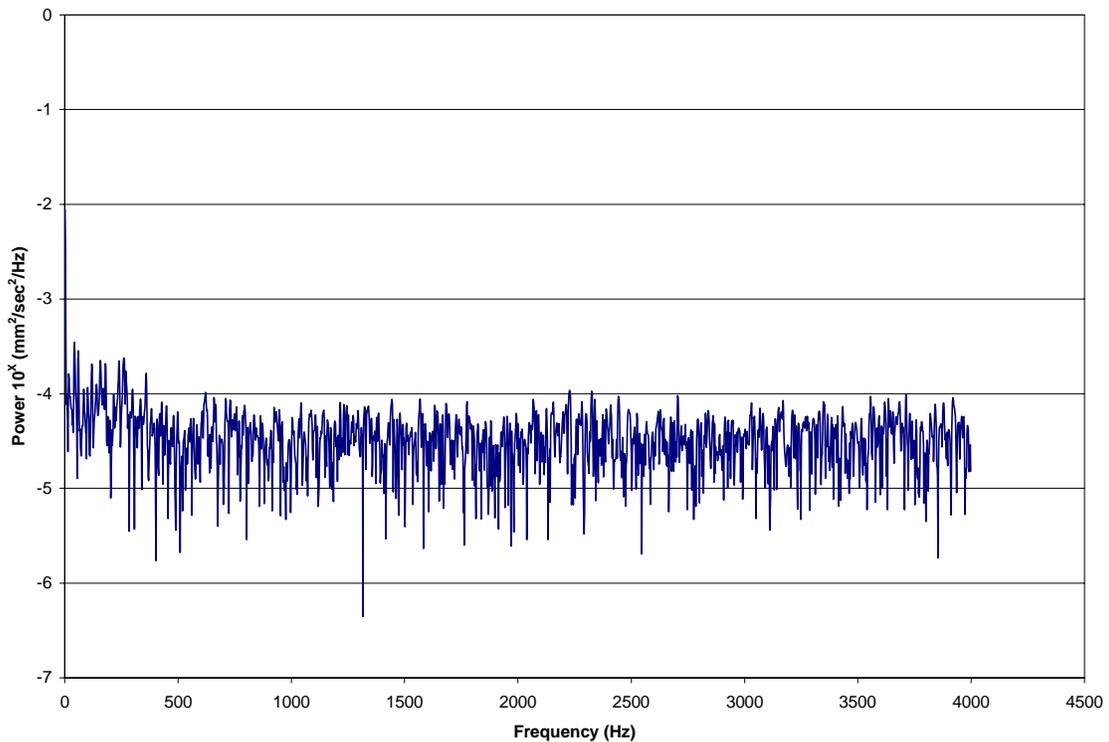
Figure 4.14: Noiseless Condition: Achieved by turning the LCOS device control box off
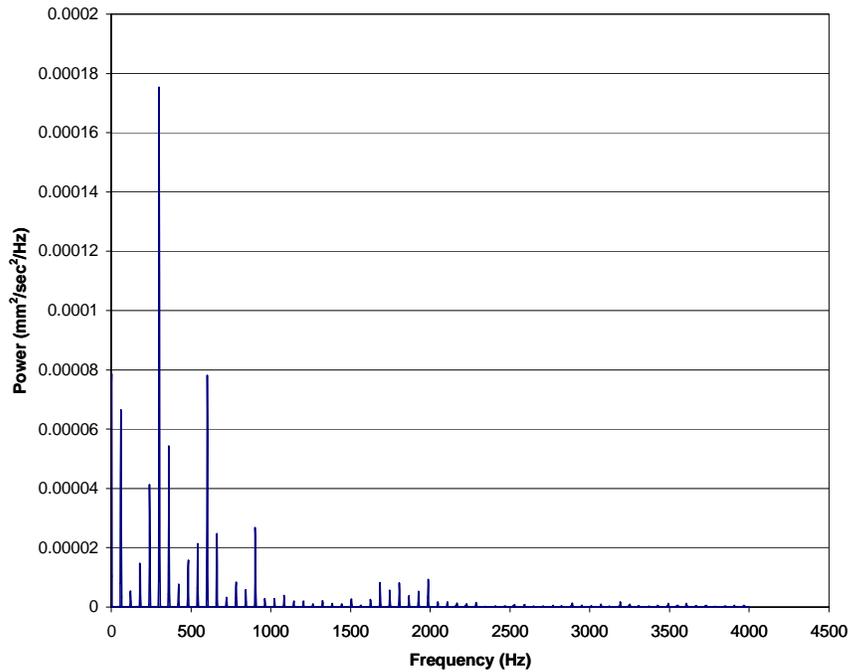
Figure 4.15: Zero Array Noise on Linear Scale: Achieved by sending the LCOS device a zero array or "black screen".

The noise spikes appearing in the power spectrums are found to be at 60Hz intervals starting at 60Hz. The dominate harmonic in the black screen image is at 300Hz. As actual steering images are applied to the LCOS device, all 60Hz harmonics rise in power with the dominate harmonics at 300Hz, 600Hz, and 900Hz as shown in figures 4.16 through 4.22.

This noise is likely electrical power and control box components. The device control box is powered with standard 120V 60Hz electricity. The update frequency for the voltages applied to the LCOS device from the control box is 60Hz. Furthermore, the polarization of the electrical field within the device is oscillated at 60Hz. The

44

polarization of the field applied to the device is oscillated to prevent a current from

building within the crystals as discussed in chapter 2. [1]
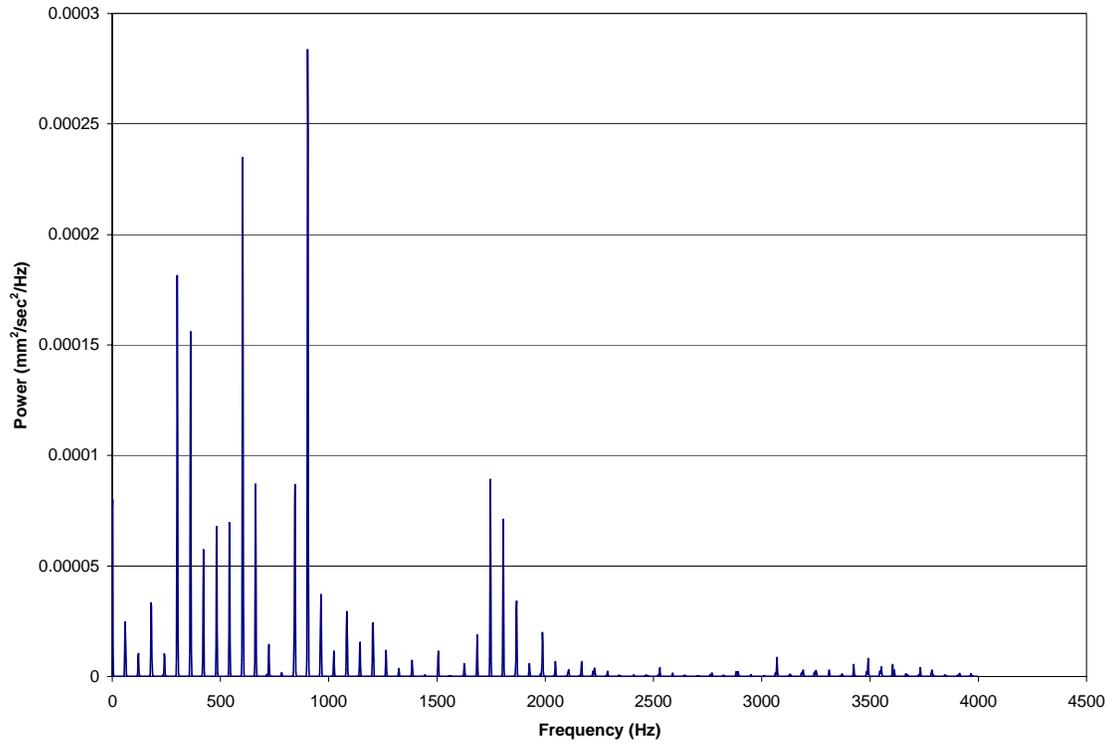
Figure 4.16: Compensation Image Noise on Linear Scale.
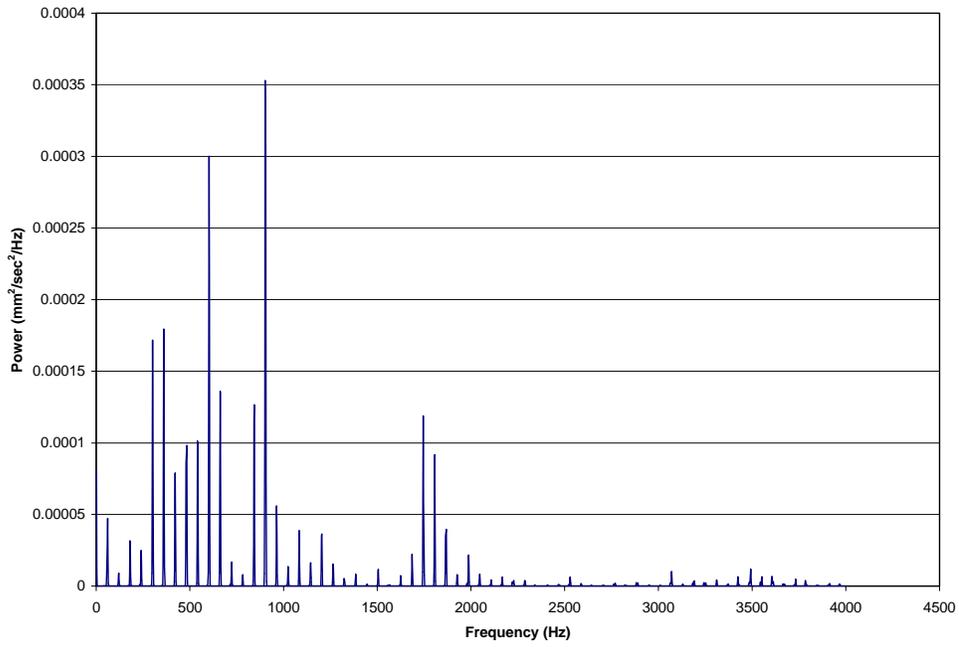
Figure 4.17: 1mrad Left Noise on Linear Scale.
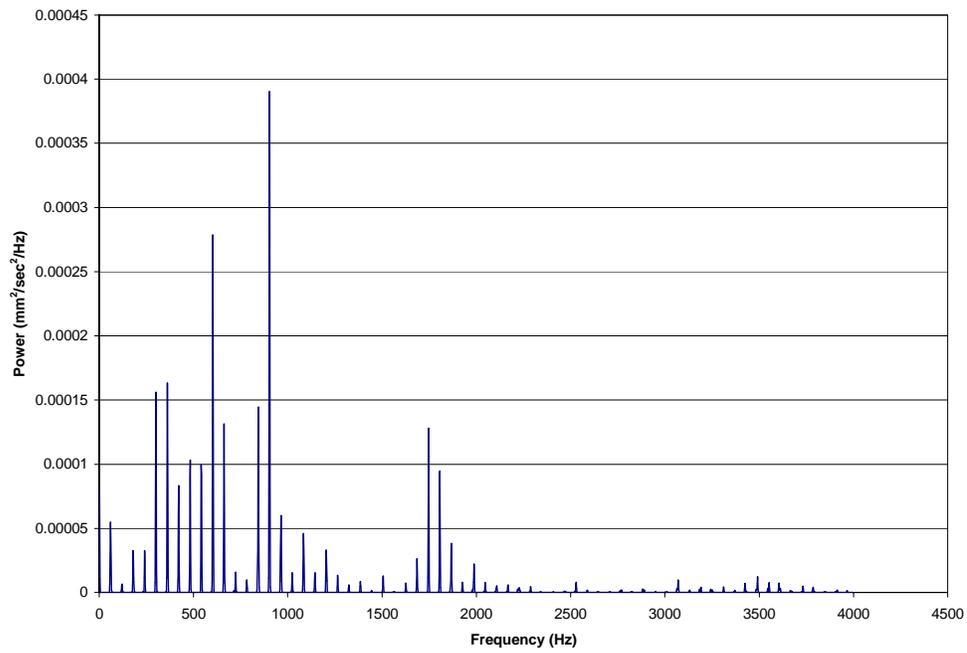
Figure 4.18: 1mrad Right Noise on Linear Scale.
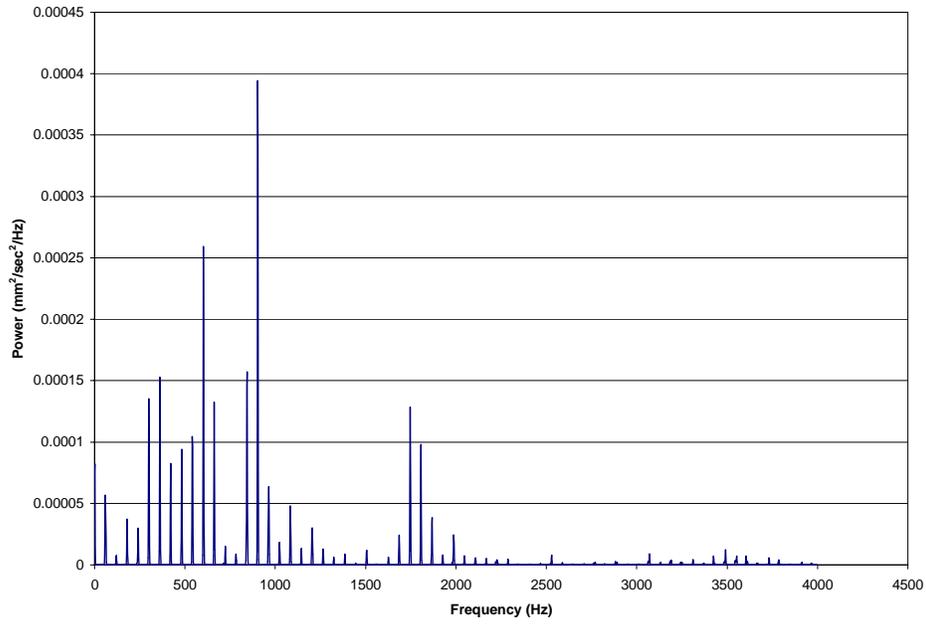
Figure 4.19: 2mrad Left Noise on Linear Scale.
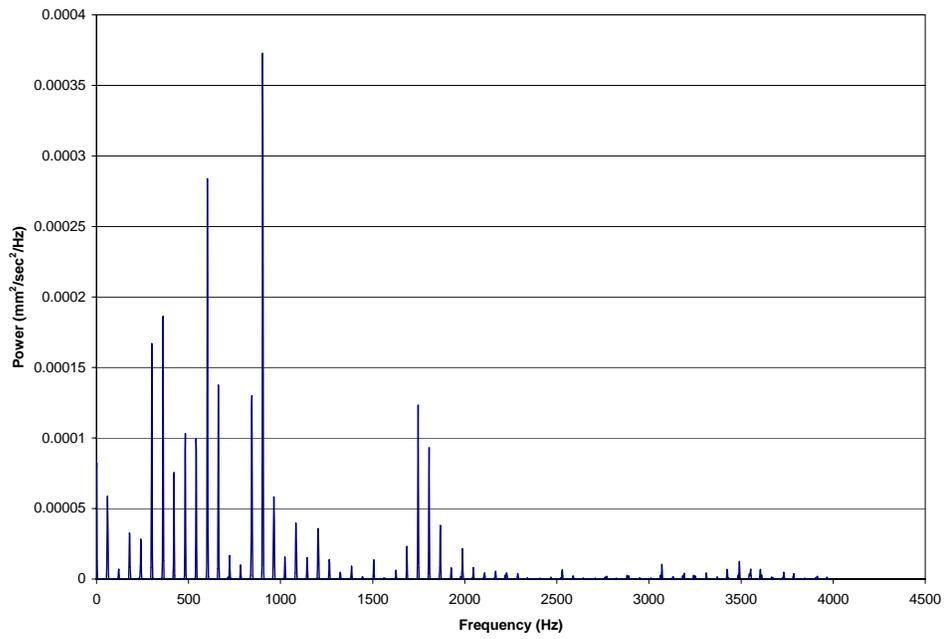
Figure 4.20: 2mrad Right Noise on Linear Scale.
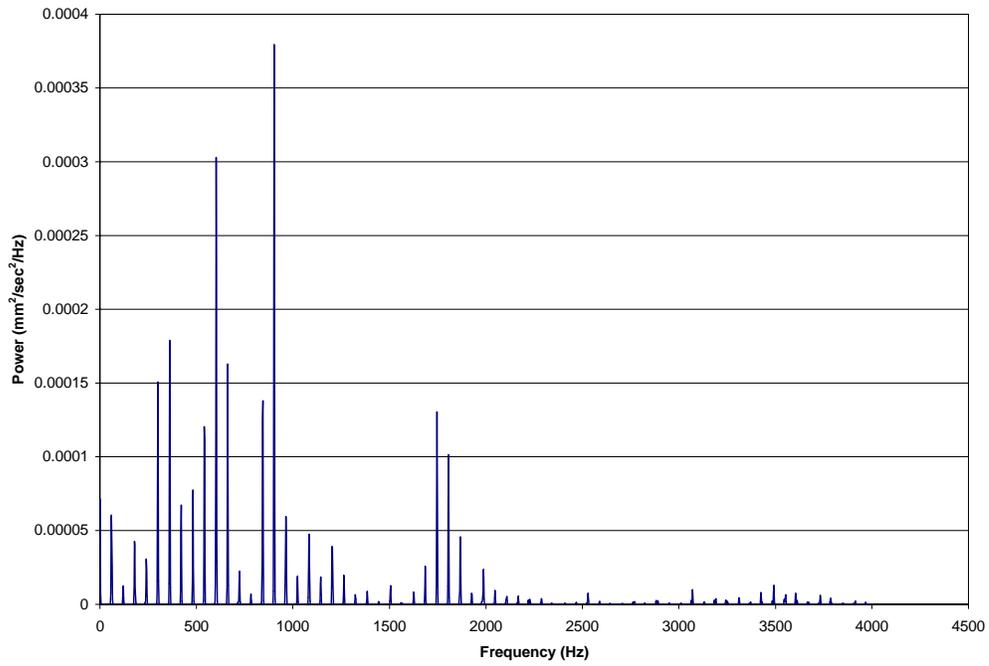
Figure 4.21: 3mrad Left Noise on Linear Scale.
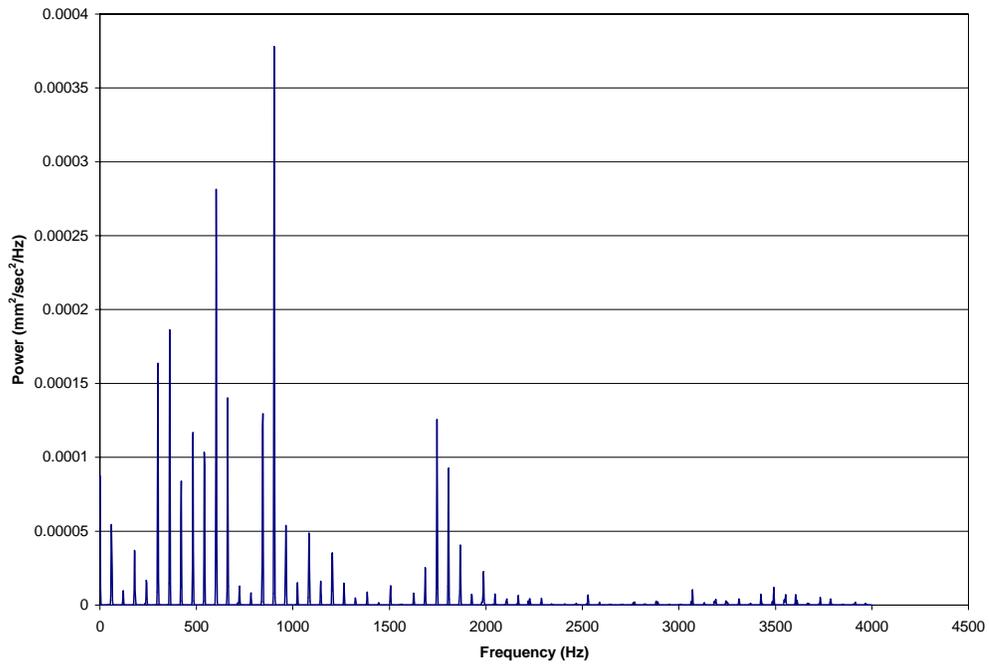
Figure 4.22: 3mrad Right Noise on Linear Scale.

The noise spectrum was found to remain relatively constant when compared to the vibration signal. The noise profile remains at the same frequencies and varies slightly in amplitude with steering angle. Therefore, it was possible to subtract the noise spectrum from a spectrum containing both a vibration target signal and noise. The result is shown in figure 4.23 below where the LVS was receiving a 1500Hz signal.
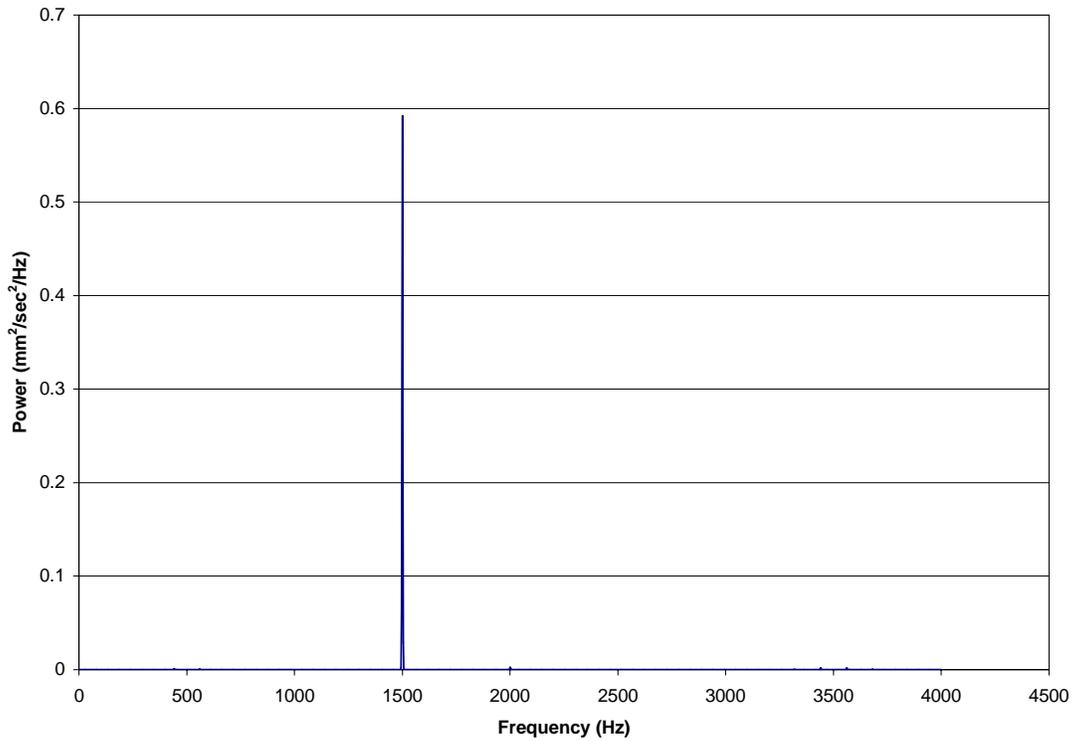
Figure 4.23: Vibration Signal Minus Noise on Linear Scale.

4.7 Split Beam Vibration Signal

It is advantageous for combat target identification and location purposes to have the capability of simultaneously measuring individual waveforms from independent vibration targets. Testing this concept, the LCOS device was used to split the incoming LVS beam into 2 separate sensor beams; simultaneously steering the left beam to 3mrad and the right beam to 3mrad. A 2500Hz signal was applied to the left beam with a frequency generating box, and a 700Hz signal was applied to the right beam with a tuning fork, creating a clear delineation between the 2 recorded target signals. Once again, all undesired diffraction orders were removed with variable apertures. The combined waveform was sampled 4096 times and the Fourier Transform shows each target signal displayed several orders of magnitude above the system noise as shown in Figure 4.24.
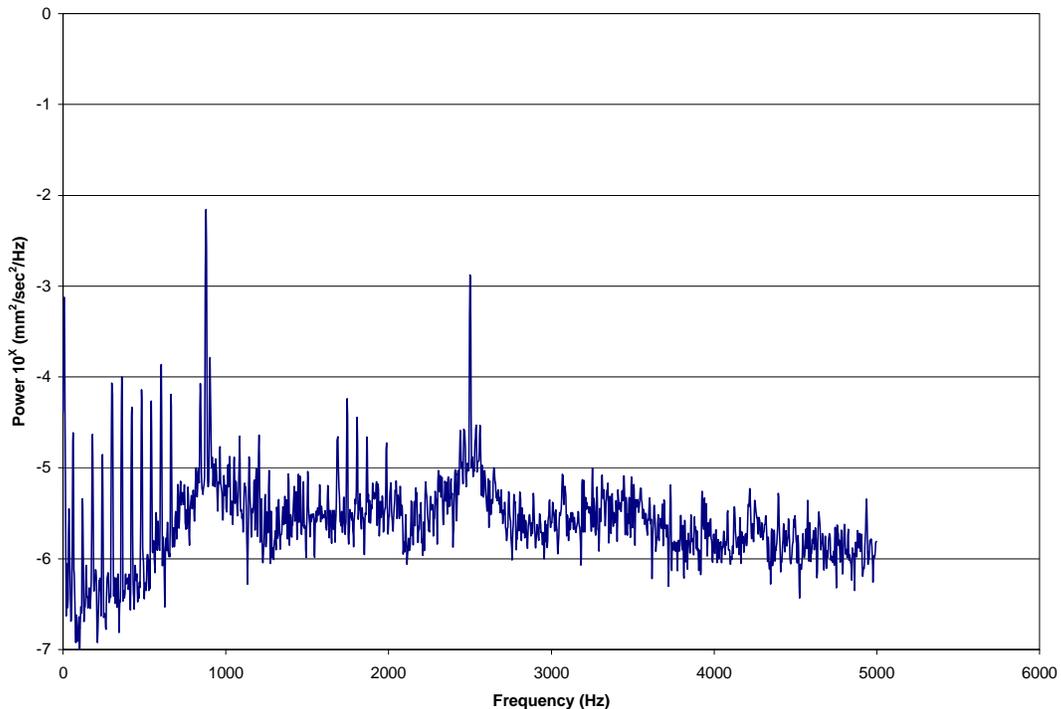
Figure 4.24: Split Beam Multiple Target Power Spectrum: LVS tracking a 2500Hz target simultaneously with a 700Hz target while the LVS beam is being split 3mrad to the right target and 3mrad to the left target by the LCOS device.

50

It is worth noting that the magnitudes of the target signals are not equal. The 2500Hz signal was provided by a frequency generator with constant amplitude. However, the amplitude of the tuning fork varied with time after the fork was struck. A best attempt was made to manually select the time to capture the combined waveform when the tuning fork amplitude approached the amplitude of the frequency generator. As the waveform in figure 4.24 continues over several more seconds, the tuning fork signal intensity drops until both signals are equal and then the frequency generator becomes the dominant amplitude.

4.8 Summary

This section addressed the results of the research test criteria. The data showed that it is possible to steer the beam of a laser vibrometer system with a non-mechanical beam steering device. However, there are future challenges that will need to be overcome to move the technology to a fielded weapon or sensing system. The polarization was found to rotate on the first pass through the device and was corrected to within a few degrees of the original polarization on the return pass. The noise induced by the device was found to be constant across steering angles and so therefore could be subtracted. The LVS successfully measured a vibration signal across the steered beam. Additionally, the LVS effectively measured two independent vibration signals simultaneously across a split beam. The next section will explain the conclusions obtained from this research effort.

V.   Conclusions

5.1 Introduction

The focus of this research effort was to develop a proof of concept for the steering of a laser vibrometer system with a non-mechanical beam steering device. The ability to steer Air Force laser radar sensor systems by non-mechanical means promises to overcome both the technical and economical shortcomings of mechanical and gimbaled mirror systems. Non-mechanical beam steering offers advantages of reduced weight, increased steering speed, beam splitting capabilities for maximum utilization of resources, and economical advantages measured in the overall increased functionality of the proposed system.

In addition, the equipment used for the experiments contained within this document was conducted with commercial off the shelf equipment (COTS). The use of COTS equipment provides both a cost and logistics advantage when compared to systems developed exclusively for the Department of Defense. Successful vibration target tracking with COTS equipment served to demonstrate the capability for developing future Air Force laser radar steering solutions from the combination and integration of commercially available components.

5.2 Assumption from research data

The LVS was used as a scaled test scenario for a laser radar steering solution. The experiments conducted during this research effort served to examine: polarization

effects induced by the LCOS device; the ability of the LVS to track a single vibration target signal while being steered by the LCOS device; the ability of the LVS to track two independent vibration target signals while the beam of the LVS was being split by the LCOS device; and a measurement of the noise introduced to the LVS signal by the LCOS device.

The linear polarization incident upon the LCOS device was found to rotate after steering. When the steered beam was reflected back through the device on the second pass, the polarization was found to return to within a few degrees of the incident polarization. A polarization challenge of special significance resulted from incompatible polarization states between the LVS and the LCOS device. The proper polarization states between the different devices' technologies were achieved using a polarizer at the expense of efficiency. This condition afforded a measurable degree of success in the experiments of this research effort. However, forcing the compatible polarization states resulted in a significant loss to the intensity of the LVS beam.

Efficiency of the combined systems was of interest during this research. As previously noted, developing a configuration that allowed the systems to be used together resulted in a reduced intensity of the vibrometry beam. Nonetheless, the low efficiencies were acceptable to achieve the goal of this research, which was to accurately receive a vibration signal over a steered vibrometry beam. Though, future design and integration efforts are required before the technology could be applied to a fielded system.

Under laboratory conditions, the LVS was able to successfully track a vibration target signal while the beam was steered by the LCOS device. The LCOS device was steered to the published extent of useful efficiency in both directions along the horizontal

axis. The vibration target signal was received at the correct frequency at each angle. The

vibration target signal was received several orders of magnitude above any system noise

generated by the LCOS device for each steering angle.

After successful steering, the LVS beam was split by the LCOS device.   Under

this condition, the LVS was able to successfully track two separate vibration target

signals simultaneously. Once again, the vibration target signals were received at the

correct frequency and several orders of magnitude above the system noise generated by

the LCOS device.

A measurement and evaluation of the system noise induced by the LCOS device

found the noise signal was generated at 60Hz intervals. This noise is attributed to the

standard 120V, 60Hz AC power due to the lack of internal shielding in the LCOS control

box. Additionally, the voltage update frequency from the control box to the LCOS

device is 60Hz; and the polarization of the electric field applied to the device is oscillated

at 60Hz. The noise was found to be consistent across steering angles and could

successfully be subtracted from the received vibration signal to produce a clear target

signal.

5.3 Research Advances and Implications

This research effort explored the possibility of combining the use of a non-

mechanical beam steering device with a coherent laser radar system. In addition, the

technologies tested were commercially available components. The results of this

research demonstrate there is great potential for using non-mechanically steering devices

to direct the beams of active sensor systems in the future. Replacing the current gimbaled steering systems with non-mechanical devices will provide benefits in speed, power consumption, weight, and beam splitting. These advantages will increase the capabilities of sensor platforms to locate and identify targets. Additionally, airborne platforms and unmanned aerial vehicles (UAVs) will specifically benefit with decreased fuel consumption and increased loiter times. Beam splitting capabilities will increase the amount of sensor data that may be captured during a sensor scan. The increased data will serve to increase the probability of detection as well as the accuracy of identification. With all of the advantages gained from non-mechanical steering devices there are still several shortcoming observed in this research. Most notably, the non-mechanical beam steering devices are limited in steering range and the polarization requirements are incompatible with the laser radar transmit/receive (TR) switch resulting in decreased efficiencies.

5.4 Recommendations for future work

Although this research was successful, the efficiency sacrifices show that the two systems are not designed to work together. A design effort to combine the systems within a single unit for maximum efficiency would allow for the exploration of many other areas of combat target identification and location. A fiber optic link between laser radar and the non-mechanical beam steering device may prove to overcome many losses attributed to the incompatible polarization states.

Additional advancements in liquid crystal technology may produce a non-polarization dependent steering device. This could allow almost immediate integration with various laser radar systems. In addition, greater steering angles are required for implementation on any operation laser radar systems. The small angles observed in this research would require large stand-off distances, optical telescopes, or sensor platform rotation to accomplish mission requirements. Any one of these concessions reverses the advantages sought from non-mechanical laser radar steering solutions.

With increased system efficiency, the LVS beam could be split into several more beams. This would open opportunities for using the LVS to probe hot spots identified by other sensing systems. The LVS may potentially have the capability to simultaneously scan several targets. A vibration signal received along any beam could then be used to identify a target as the frequency "vibration signature" of the target is likely unique to a specific vehicle or mechanical device. Further research is required to develop the capability of determining the beam that each frequency is received on. This capability would provide a complete combat target identification and location profile. Combining these improvements with the successes within this research effort demonstrates great potential for using non-mechanical beam steering devices as a future Air Force laser radar steering solution.

Appendix A. MATLAB steering phase image generation

A.1 Introduction

The HANA Liquid Crystal on Silicon non-mechanical beam steering device operates by receiving pixel voltages from the LCOS control box. The control box receives grayscale values from 0-255 for each pixel from a standard computer monitor an assigns each value an appropriate voltage. The grayscale images are representative of phase ramps necessary for the steering of the incident wavefront.

A.2 Compensation image only (0mrad steering)

The MATLAB code below applies the compensation image and electro-optical response curve to the device without a steering phase ramp

```
% Capt Kevin Kuciapinski
% HANA Device
% Compensation image only 0rad steering
%
k=0;
img=zeros(768,1024);
load('compsurf.mat');
adjsurf2=-1*surf2';
for i=1:768;
   for j=1:1024;
      correctedsurf(i,j)=adjsurf2((768-(i-1)),j);
   end;
end;
correctedimg=img+correctedsurf;
finalimg=mod(correctedimg,1);
```

```
z=finalimg;
figure(1);
title('No Ramps + Surf2');
plot(z(1,:));
for j=1:1024;
    for i=1:768
    z(i,j)=-82.521*z(i,j)^4+425.35*z(i,j)^3-484.048*z(i,j)^2-49.964*z(i,j)+213.9;
    end;
end;
%figure (8);
%colormap(gray);
%map=colormap;
%imagesc(z);
img=uint8(z);
imwrite(img, 'adjsurf.bmp')  %save with correct colormap
```

A.3 Steering 1mrad Right

The MATLAB code below applies the compensation image and electro-optical response curve to the device with a steering phase ramp for 1mrad Right

```
% Capt Kevin Kuciapinski
% HANA Device
% Steering 1mrad Right
%
k=31.65;
img=zeros(768,1024);
load('compsurf.mat');
adjsurf2=-1*surf2';
for i=1:768;
    for j=1:1024;
```

```
      correctedsurf(i,j)=adjsurf2((768-(i-1)),j);
   end;
end;
%  for i=1:768,img(i,:)=255*rem(1:1024,k)'/k;
for i=1:768
   img(i,:)=rem(1:1024,k)/k;
   %  img(i,:)=255*(rem(1024:-1:1,k)/k);
end;
correctedimg=img+correctedsurf;
finalimg=mod(correctedimg,1);
z=finalimg;
figure(1);
title('Ramps + Surf2');
plot(z(1,:));
for j=1:1024;
   for i=1:768
   z(i,j)=-82.521*z(i,j)^4+425.35*z(i,j)^3-484.048*z(i,j)^2-49.964*z(i,j)+213.9;
   end;
end;
figure (2);
colormap(gray);
%map=colormap;
imagesc(z);
img=uint8(z);
imwrite(img,'1mrad.bmp')  %save with correct colormap
```

A.4 Steering 2mrad Right

The MATLAB code below applies the compensation image and electro-optical response curve to the device with a steering phase ramp for 2mrad Right.

```matlab
% Capt Kevin Kuciapinski
% HANA Device
% Steering 2mrad Right
%
k=15.825;
img=zeros(768,1024);
load('compsurf.mat');
adjsurf2=-1*surf2';
for i=1:768;
    for j=1:1024;
        correctedsurf(i,j)=adjsurf2((768-(i-1)),j);
    end;
end;
%   for i=1:768,img(i,:)=255*rem(1:1024,k)'/k;
for i=1:768
    img(i,:)=rem(1:1024,k)/k;
    %   img(i,:)=255*(rem(1024:-1:1,k)/k);
end;
correctedimg=img+correctedsurf;
finalimg=mod(correctedimg,1);
z=finalimg;
figure(1);
title('Ramps + Surf2');
plot(z(1,:));
for j=1:1024;
    for i=1:768
    z(i,j)=-82.521*z(i,j)^4+425.35*z(i,j)^3-484.048*z(i,j)^2-49.964*z(i,j)+213.9;
    end;
end;
```

```
figure (8);
colormap(gray);
%map=colormap;
imagesc(z);
img=uint8(z);
imwrite(img,'2mrad.bmp')  %save with correct colormap
```

A.5 *Steering 3mrad Right*

The MATLAB code below applies the compensation image and electro-optical response curve to the device with a steering phase ramp for 3mrad Right.

```
% Capt Kevin Kuciapinski
% HANA Device
% Steering 3mrad Right
%
k=10.55;
img=zeros(768,1024);
load('compsurf.mat');
adjsurf2=-1*surf2';
for i=1:768;
   for j=1:1024;
      correctedsurf(i,j)=adjsurf2((768-(i-1)),j);
   end;
end;
%  for i=1:768,img(i,:)=255*rem(1:1024,k)'/k;
for i=1:768
   img(i,:)=rem(1:1024,k)/k;
   %  img(i,:)=255*(rem(1024:-1:1,k)/k);
end;
```

```matlab
correctedimg=img+correctedsurf;
finalimg=mod(correctedimg,1);
z=finalimg;
figure(1);
title('Ramps + Surf2');
plot(z(1,:));
for j=1:1024;
    for i=1:768
    z(i,j)=-82.521*z(i,j)^4+425.35*z(i,j)^3-484.048*z(i,j)^2-49.964*z(i,j)+213.9;
    end;
end;
figure (2);
colormap(gray);
%map=colormap;
imagesc(z);
img=uint8(z);
imwrite(img,'3mrad.bmp')  %save with correct colormap
```

A.6 Steering 1mrad Left

The MATLAB code below applies the compensation image and electro-optical response curve to the device with a steering phase ramp for 1mrad Left.

```matlab
% Capt Kevin Kuciapinski
% HANA Device
% Steering 1mrad Left
%
k=31.65;
img=zeros(768,1024);
load('compsurf.mat');
adjsurf2=-1*surf2';
```

```matlab
for i=1:768;
   for j=1:1024;
      correctedsurf(i,j)=adjsurf2((768-(i-1)),j);
   end;
end;
%  for i=1:768,img(i,:)=255*rem(1:1024,k)'/k;
for i=1:768
   img(i,:)=rem(1:1024,k)/k;
   %  img(i,:)=255*(rem(1024:-1:1,k)/k);
end;
correctedimg=fliplr(img)+correctedsurf;
finalimg=mod(correctedimg,1);
z=finalimg;
figure(1);
title('Ramps + Surf2');
plot(z(1,:));
for j=1:1024;
   for i=1:768
   z(i,j)=-82.521*z(i,j)^4+425.35*z(i,j)^3-484.048*z(i,j)^2-49.964*z(i,j)+213.9;
   end;
end;
figure (2);
colormap(gray);
imagesc(z);
img=uint8(z);
imwrite(img,'file.bmp')
```

A.7 Steering 2mrad Left

The MATLAB code below applies the compensation image and electro-optical response curve to the device with a steering phase ramp for 2mrad Left.

```matlab
% Capt Kevin Kuciapinski
% HANA Devive
% Steering 2mrad Left
%
k=15.825;
img=zeros(768,1024);
load('compsurf.mat');
adjsurf2=-1*surf2';
for i=1:768;
    for j=1:1024;
        correctedsurf(i,j)=adjsurf2((768-(i-1)),j);
    end;
end;
%  for i=1:768,img(i,:)=255*rem(1:1024,k)'/k;
for i=1:768
    img(i,:)=rem(1:1024,k)/k;
    %  img(i,:)=255*(rem(1024:-1:1,k)/k);
end;
correctedimg=fliplr(img)+correctedsurf;
finalimg=mod(correctedimg,1);
z=finalimg;
figure(1);
title('Ramps + Surf2');
plot(z(1,:));
for j=1:1024;
    for i=1:768
    z(i,j)=-82.521*z(i,j)^4+425.35*z(i,j)^3-484.048*z(i,j)^2-49.964*z(i,j)+213.9;
    end;
end;
```

```
figure (2);
colormap(gray);
imagesc(z);
img=uint8(z);
imwrite(img,'2mradLnew.bmp')
```

A.8 Steering 3mrad Left

The MATLAB code below applies the compensation image and electro-optical response curve to the device with a steering phase ramp for 3mrad Left.

```
% Capt Kevin Kuciapinski
% HANA Devive
% Steering 3mrad Left
%
k=10.55;
img=zeros(768,1024);
load('compsurf.mat');
adjsurf2=-1*surf2';
for i=1:768;
   for j=1:1024;
      correctedsurf(i,j)=adjsurf2((768-(i-1)),j);
   end;
end;
%  for i=1:768,img(i,:)=255*rem(1:1024,k)'/k;
for i=1:768
   img(i,:)=rem(1:1024,k)/k;
   %  img(i,:)=255*(rem(1024:-1:1,k)/k);
end;
correctedimg=fliplr(img)+correctedsurf;
```

```
finalimg=mod(correctedimg,1);
z=finalimg;
figure(1);
title('Ramps + Surf2');
plot(z(1,:));
for j=1:1024;
    for i=1:768
    z(i,j)=-82.521*z(i,j)^4+425.35*z(i,j)^3-484.048*z(i,j)^2-49.964*z(i,j)+213.9;
    end;
end;
figure (2);
colormap(gray);
imagesc(z);
img=uint8(z);
imwrite(img,'3mradLnew.bmp')
```

A.9 Beam Split

The MATLAB code below applies the compensation image and electro-optical response curve to the device with a split steering phase ramp for 3mrad in each direction.

```
% Capt Kevin Kuciapinski
% HANA Device
% Beam Split
%
k=10.55;
img=zeros(768,1024);
load('compsurf.mat');
adjsurf2=-1*surf2';
for i=1:768;
    for j=1:1024;
```

```matlab
        correctedsurf(i,j)=adjsurf2((768-(i-1)),j);
    end;
end;
val=rem(1:1024,k)/k;
flipval=fliplr(rem(1:1024,k)/k);
for j=1:1024;
    if j>512
        for i=1:768
            img(i,j)=val(j);
        end
%        for i=1:768
%            img(:,j)=rem(1:1024,k)/k;
%        end;
    else
        for i=1:768
            img(i,j)=flipval(j);
        end
%        for i=1:768
%            img(:,j)=rem(1:1024,k)/k;
%            img(:,j)=fliplr(img(i,j));
%        end;
    end;
end;
correctedimg=img+correctedsurf;
finalimg=mod(correctedimg,1);
z=finalimg;
figure(1);
title('Ramps + Surf2');
plot(z(1,:));
for j=1:1024;
```

```matlab
    for i=1:768
    z(i,j)=-82.521*z(i,j)^4+425.35*z(i,j)^3-484.048*z(i,j)^2-49.964*z(i,j)+213.9;
    end;
end;
figure (2);
colormap(gray);
imagesc(z);
img=uint8(z);
imwrite(img,'Vert3mradbeamsplit.bmp')
```

A.10 Black Screen (no compensation image, no steering)

The MATLAB code below applies a black screen image and electro-optical response curve to the device without a steering phase ramp or the compensation image.

```matlab
% Capt Kevin Kuciapinski
% HANA Device
% Black screen (no streeing, no compensation)



%k=0.00001;
img=zeros(768,1024);
img=uint8(img);
imwrite(img,'norampsnocomp.bmp')  %save with correct colormap;
break
%load('compsurf.mat');
%adjsurf2=-1*surf2'*0.00001;
%for i=1:768;
    for j=1:1024;
        correctedsurf(i,j)=adjsurf2((768-(i-1)),j);
    end;
```

```
end;
%  for i=1:768,img(i,:)=255*rem(1:1024,k)'/k;
for i=1:768
    img(i,:)=rem(1:1024,k)/k;
    %  img(i,:)=255*(rem(1024:-1:1,k)/k);
end;
correctedimg=img+correctedsurf;
finalimg=mod(correctedimg,1);
z=finalimg;

for j=1:1024;
    for i=1:768
    z(i,j)=-82.521*z(i,j)^4+425.35*z(i,j)^3-484.048*z(i,j)^2-49.964*z(i,j)+213.9;
    end;
end;
figure (8);
colormap(gray);
%map=colormap;
imagesc(z);
img=uint8(z);
imwrite(img,'norampsnocomp.bmp')  %save with correct colormap
```

Bibliography

1. Anderson, Jim. Design Engineer. Hana Microdisplay Technologies Inc. Telephone Interview. July 2005.

2. Boyd, Robert W. *Nonlinear Optics.* Academic Press, San Diego, CA, second edition, 2003.

3. Hecht, Eugene. *Optics.* Addison Wesley, fourth edition, 2002.

4. Jelalian, Albert V. *Laser Radar Systems*, Artech House, 1992

5. Karim, Mohammad. *Electro-Optical Devices and Systems.* PWS-Kent Publishing Company, Boston, 1990.

6. Palmer, Christopher. *Diffraction Grating Handbook.* Thermal RGL, fifth edition. April 2000.

7. Polytech. "Laser Doppler Vibrometer." User Manual. OFV-3001. Polytec GmbH. D-76337 Waldbronn.

8. Polytec. "Principles of Vibrometery." Polytec GmbH. D-76337 Waldbronn. http://www.polytec.com. June 2005.

9. Polytec. "Vibrometer University" Polytec GmbH. D-76337 Waldbronn. http://www.polytec.com. June 2005.

10. Shapiro, Jeffrey. "Target-reflection theory for coherent laser radars" *Selected Papers on Laser Radar,* SPIE Milestone Series, Vol MS 133. SPIE Optical Engineering Press, Bellingham 1997.

11. Vibrometer University. "Vibrometry Basics." Polytec GmbH. D-76337 Waldbronn. http://www.polytec.com. June 2005.

12. Wang, Xinghua Wang, Wang Bin. "LCOS Wavefront Corrector and Very Fine Beam Steerer Demo Unit Manual." Liquid Crystal Institute, Kent State University, Manual for DARPA and AFRL.

REPORT DOCUMENTATION PAGE

Form Approved
OMB No. 074-0188

The public reporting burden for this collection of information is estimated to average 1 hour per response, including the time for reviewing instructions, searching existing data sources, gathering and maintaining the data needed, and completing and reviewing the collection of information. Send comments regarding this burden estimate or any other aspect of the collection of information, including suggestions for reducing this burden to Department of Defense, Washington Headquarters Services, Directorate for Information Operations and Reports (0704-0188), 1215 Jefferson Davis Highway, Suite 1204, Arlington, VA 22202-4302. Respondents should be aware that notwithstanding any other provision of law, no person shall be subject to an penalty for failing to comply with a collection of information if it does not display a currently valid OMB control number.
PLEASE DO NOT RETURN YOUR FORM TO THE ABOVE ADDRESS.

1. REPORT DATE *(DD-MM-YYYY)* Sept 2005	2. REPORT TYPE **Master's Thesis**	3. DATES COVERED *(From – To)* Sept 2003 – August 2005

4. TITLE AND SUBTITLE Liquid Crystal on Silicon Non-Mechanical Steering of a Laser Vibrometer System	5a. CONTRACT NUMBER
	5b. GRANT NUMBER
	5c. PROGRAM ELEMENT NUMBER
6. AUTHOR(S) Kuciapinski, Kevin, S., Captain, USAF	5d. PROJECT NUMBER
	5e. TASK NUMBER
	5f. WORK UNIT NUMBER

7. PERFORMING ORGANIZATION NAMES(S) AND ADDRESS(S) Air Force Institute of Technology Graduate School of Engineering and Management (AFIT/EN) 2950 Hobson Way WPAFB OH 45433-7765	8. PERFORMING ORGANIZATION REPORT NUMBER AFIT/GSS/ENP/05-01
9. SPONSORING/MONITORING AGENCY NAME(S) AND ADDRESS(ES) AFRL/SNJM Attn: Mr. Robert J. Feldmann 3109 Hobson Way, Bldg 622 WPAFB OH 45433-7700 DSN: 785-9614 x232	10. SPONSOR/MONITOR'S ACRONYM(S)
	11. SPONSOR/MONITOR'S REPORT NUMBER(S)

12. DISTRIBUTION/AVAILABILITY STATEMENT
   APPROVED FOR PUBLIC RELEASE; DISTRIBUTION UNLIMITED.

13. SUPPLEMENTARY NOTES

14. ABSTRACT
This research examined the possibility of using a non-mechanical beam steering device to steer the beam of a coherent laser radar system. Non-mechanical beam steering devices offer many advantages in size, weight, power requirements, and steering speeds. Additionally, non-mechanical beam steering devices present the capabilities of splitting a single beam into multiple beams as well as beam forming and expanding. The coherent laser radar system used was a Laser Vibrometer System. The beam of the laser vibrometer was steered from 0 mrad to 3 mrad at 1 mrad increments using the liquid crystal on silicon (LCOS) device. The laser vibrometer was able to accurately measure a 2500 Hz vibration target on the steered vibrometry beam at all steered angles. A small LCOS noise signal was detected. The LCOS noise spectrum was determined to be consistent and predictable located at 60 Hz harmonics and was successfully subtracted from the signal. The LCOS device was used to split the vibrometry beam into 2 separate beams. The vibrometer was able to accurately measure two simultaneous independent target signals over the split beam.

15. SUBJECT TERMS
Beam Steering, Beam Splitting, Laser Vibrometry, LVS, Optical Phased Array, OPA, Liquid Crystal on Silicon, LCOS, Laser Radar, Coherent Laser Radar

16. SECURITY CLASSIFICATION OF:			17. LIMITATION OF ABSTRACT	18. NUMBER OF PAGES	19a. NAME OF RESPONSIBLE PERSON Thomas Alley, Lt Col, USAF (ENP)
REPORT **U**	ABSTRACT **U**	c. THIS PAGE **U**	**UU**	84	19b. TELEPHONE NUMBER *(Include area code)* (937) 255-6565, ext 7290; email: Thomas.Alley@afit.edu

Standard Form 298 (Rev: 8-98)
Prescribed by ANSI Std. Z39-18